energies

MDPI

Article

Temporal and Spatial Coordination of Photovoltaic Electricity on Mountain Expressways: Battery Storage Versus Service Area–Tunnel Interconnection

Dajian Dong [1], Yongxing Wang [1], Yue Tong [1], Guie Shi [2,3,*], Anping Wang [1], Qin Qin [2,3], Hongbo Shu [2,3] and Yanchun Xu [4]

[1] Yunnan Xuanhui Expressway Co., Ltd., Qujing 654299, China; 18213496315@163.com (D.D.); lanjia84@126.com (Y.W.); tongyue2014@yeah.net (Y.T.); 18787475350@139.com (A.W.)
[2] School of Highway and Construction Engineering, Yunnan Jiaotong Polytechnic University, Kunming 650500, China; 2004070259@ynjtc.edu.cn (Q.Q.); shuhongbo2000@163.com (H.S.)
[3] Yunnan Province Education Department Plateau Infrastructure Intelligent Construction Engineering Research Center, Kunming 650500, China
[4] College of Electrical Engineering & New Energy, China Three Gorges University, Yichang 443002, China; xyc7309@163.com
* Correspondence: 2025080101@ynjtc.edu.cn

Abstract

Mountain expressways combine fragmented photovoltaic (PV) deployment spaces with spatially separated electricity demands. This study compares battery storage and electricity transfer between the Zhehai service area and Xiniushan Tunnel in Yunnan, China. A representative year of 8760 hourly records was reconstructed from annual and monthly energy constraints. Five equipment configurations, including two dispatch priorities for the combined system, were evaluated using hourly energy accounting, 25-year cash flows and carbon screening. With 608 kWp of PV and 904.0 MWh annual generation, isolated PV used only 18.3% locally. A 335 kWh battery added 92.8 MWh of useful renewable supply, whereas a 0.65 km tunnel connection added 386.8 MWh. Tunnel-first dispatch in the combined system achieved 69.8% PV self-consumption and 52.9% corridor self-sufficiency. PV alone had the highest NPV, CNY 1.013 million, while the combined tunnel-first configuration remained negative at CNY −0.165 million. External Guangxi load profiles preserved the connection's utilization advantage but reversed its economic ranking relative to local storage. Grid decarbonization and component emission proxies reduced estimated carbon benefits. These model-based results support staged investment, with connection and storage assessed separately against coincident demand, additional costs and local operating conditions.

Keywords: mountain expressway; photovoltaic self-consumption; battery energy storage; cross-node energy coordination; tunnel load

Check for updates

Academic Editor: King Jet Tseng

Received: 30 August 2026
Revised: 23 October 2026
Accepted: 4 November 2026
Published: 7 November 2026

Copyright: © 2026 by the authors. Licensee MDPI, Basel, Switzerland. This article is an open access article distributed under the terms and conditions of the Creative Commons Attribution (CC BY) license.

1. Introduction

The rapid electrification of transportation infrastructure and the increasing penetration of renewable energy are reshaping expressways from conventional transport corridors into linear energy systems [1]. In addition to traditional loads such as lighting, monitoring, tolling, communication, and tunnel operation, expressways are facing growing electricity demand from electric vehicle charging, commercial facilities in service areas, and intelligent traffic systems [2]. This transition creates opportunities for reducing operational carbon emissions, but also brings challenges for energy planning because renewable generation

and electricity demand are unevenly distributed along long-distance corridors [3]. These challenges are particularly prominent in mountain expressways, where service areas, tunnels, slopes, interchanges, central medians, rooftops, carports, and tunnel portals jointly form a fragmented right-of-way environment [4,5]. Under such conditions, renewable energy planning cannot be reduced to maximizing photovoltaic or wind power capacity at isolated sites [6]. A service area with sufficient rooftop or carport space may still experience poor self-consumption due to the temporal mismatch between solar generation and local demand [7], while a nearby tunnel may have a large and continuous electricity demand but is rarely considered a load sink for surplus renewable electricity [8]. Therefore, the key practical demand is to organize scattered renewable resources and heterogeneous load nodes into a coordinated energy supply system [9].

Existing studies have established an important foundation for renewable energy utilization in highway systems [10]. On the demand side, load characterization has gradually shifted from empirical estimation to data-driven and time-series modeling. Historical electricity consumption, traffic flow, meteorological variables, charging behavior, and operational information have been incorporated to describe intra-day fluctuations, seasonal variations, and long-term growth trends in service area loads [11]. For tunnels, energy consumption models have been developed for lighting [12], ventilation [13,14], monitoring, and safety-related equipment, with increasing attention paid to the effects of traffic flow, tunnel length, luminance requirements, and ventilation control strategies. On the supply side, photovoltaic and wind energy applications along highways have been widely investigated [15], including BIM–GIS-based photovoltaic site selection [16,17], service area rooftop PV, parking canopy PV [18], PV noise barriers, PV optimization [19], slope PV [20], tunnel entrance canopies, road space PV systems [21,22], roadside wind environments, tunnel portal wind acceleration, and small-scale wind turbines under specific topographic conditions [23]. More recently, highway energy system studies have extended from single renewable generation systems to PV storage systems [24], including integrated rest-area PV storage schemes [25] and simultaneous capacity–schedule optimization for PV-BESS charging stations [26,27], hybrid solar–wind systems [28–30], highway ring multi-microgrids with fixed/mobile storage [31] and virtually networked multi-node energy systems [32]. These studies indicate that storage and coordinated source–load scheduling can improve renewable electricity utilization and reduce grid dependence [33,34]. These studies also suggest that the performance of highway renewable energy systems depends not only on installed capacity, but also on the temporal matching between renewable generation and heterogeneous load demand [35].

Despite these advances, the applicability of existing approaches to mountain expressway energy planning remains limited in several aspects. First, demand identification, renewable resource assessment, and system configuration are often conducted as separate tasks. As a result, the need for storage or cross-node coordination is not always directly explained by actual load profiles, and renewable energy deployment is not always constrained by local resource and space conditions. Second, studies mainly address individual service areas or charging stations [36–39], or multi-microgrid coordination [40,41], while the potential complementarity between stochastic service area loads and continuous tunnel loads has received limited attention, even though these nodes may be spatially adjacent and functionally coupled in mountain corridors. Third, regional renewable resource data may not fully represent practical deployment potential under mountain conditions, where terrain effects and fragmented usable spaces can affect the feasibility of PV and wind energy utilization [42]. These gaps leave an unresolved engineering question: under limited project data, how much additional renewable electricity can be used by adding storage, and

how much can be used by coordinating a service area supply node with a nearby tunnel demand node?

To address this question, the Xuanwei–Huize Expressway in Yunnan Province, China, is examined as a representative mountain corridor case in this study. A deterministic representative-year data set is reconstructed by applying energy-constrained normalization to the reported annual and monthly totals. The reconstructed series are used for comparative scenario evaluation and are not presented as monitored historical data. Resource evidence is also used as a deployment constraint: PV is included because installed capacity and monthly generation are reported, whereas wind generation is excluded from the evidence-based scenarios because no project-specific turbine configuration or validated generation series is available.

Five configurations are evaluated under the same service-area-plus-tunnel accounting boundary: grid supply (S0), service area PV (S1), local PV with battery storage (S2), PV with a service area/tunnel connection (S3), and PV with both battery storage and cross-node connection (S4). The combined configuration is evaluated with battery-first (S4-B) and tunnel-first (S4-T) surplus allocation. The study has three objectives: (1) to reconstruct energy-consistent hourly profiles and identify the chronological mismatch among service area demand, tunnel demand, and PV generation; (2) to distinguish the temporal shifting contribution of battery storage from the spatial coordination contribution of the continuous tunnel load; and (3) to compare the technical, grid-related carbon, and 25-year economic performance of the five configurations under a common boundary and identify the assumptions that govern their transferability. The contribution is therefore not a new forecasting or optimization algorithm, but a transparent, data-status-aware framework that links resource suitability, heterogeneous load characteristics, hourly energy flow accounting, and lifecycle decision indicators. This framework provides case-based evidence on when storage, cross-node coordination, or staged implementation is more appropriate for a mountain expressway (Figure 1).

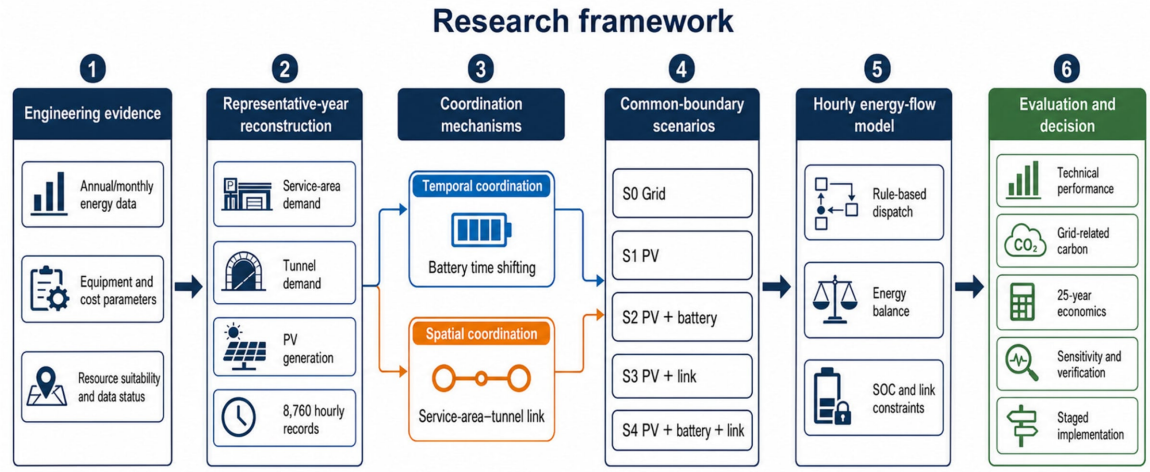


Figure 1. The research framework of this work.

2. Case Description and Methodological Framework

This section introduces the engineering case, selected analysis nodes, and data basis of the study, followed by the methodological framework used for demand assessment, renewable resource evaluation, scheme setting, and performance comparison. The purpose is to establish a clear link between the mountain expressway case conditions and the subsequent evaluation of cross-scenario PV–battery–load coordination.

2.1. Description of Study Area and Selected Nodes

The Xuanwei–Huize Expressway in Yunnan Province, southwestern China, was selected as a mountain expressway case. The route is 96.74 km long, with tunnels accounting for approximately 45% of its length, and includes one service area and two parking areas. PV installation spaces and electricity demand nodes are distributed along the route, motivating a comparison between local battery storage and electricity transfer between nearby facilities.

The Zhehai service area and Xiniushan Tunnel were selected as the two nodes within the study boundary (Figure 2). The service area is located at 26.49° N, 103.62° E and provides approximately 2039 m^2 of usable rooftop area and 1200 m^2 of carport area, totaling 3239 m^2 for PV deployment. Its projected PV capacity of 608 kWp was adopted as the reference configuration, with an annual generation input of 904.0 MWh. The reference annual service area demand was 300.0 MWh. These annual quantities were used as energy constraints for reconstructing hourly profiles. The left and right bores of Xiniushan Tunnel are approximately 2417 and 2370 m long, respectively. Its reference annual electricity demand is 892.6 MWh, dominated by lighting and ventilation, approximately 2.98 times the service area demand. The selected nodes are approximately 600–700 m apart; an equivalent link length of 0.65 km was adopted for the scenario analysis. Their proximity and different demand characteristics provide a basis for examining whether daytime PV surplus can be transferred from the service area to the tunnel.

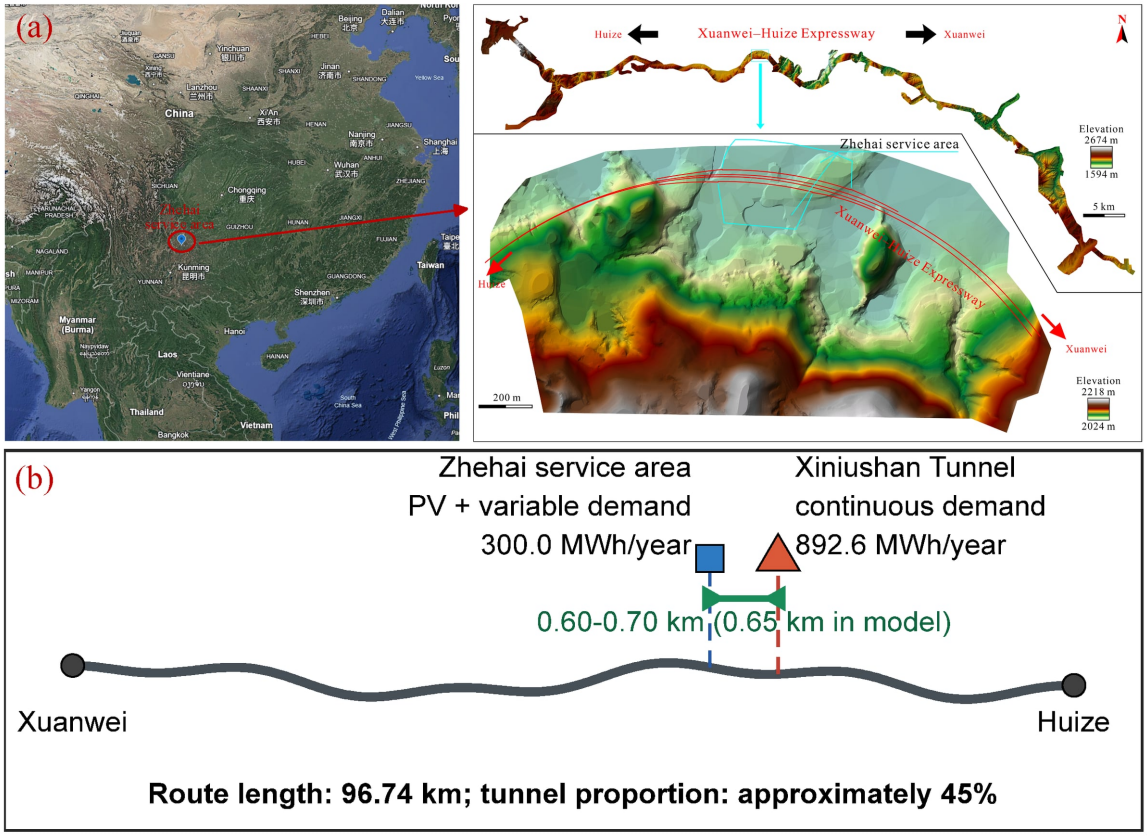


Figure 2. Location information of Xuanwei–Huize Expressway and Zhehai service area. (**a**) Geographic location of Xuanwei–Huize Expressway and Zhehai service area. (**b**) Variable demand of Zhehai service area and continuous demand of Xiniushan Tunnel.

A project battery capacity of 335 kWh was adopted as the reference storage size. With the assumed SOC range of 10–90% and a 0.5 C charge/discharge limit, this corresponds to a usable storage window of 268 kWh and a nominal power limit of 167.5 kW. A reference input power limit of 500 kW was used for the interconnection. The reference capac-

ities provide a consistent basis for comparing configurations, while sensitivity analyses vary PV capacity, battery capacity and transfer power to assess their technical effects and economic implications.

2.2. Reconstruction of Representative-Year Hourly Profiles

The supplied engineering materials contain annual or monthly energy quantities, selected daily operating characteristics, and equipment capacities, but do not contain simultaneous measured time series for the service area, Xiniushan Tunnel, and photovoltaic (PV) system. Therefore, a deterministic representative-year data set with 8760 hourly records was reconstructed. The purpose of this reconstruction is to preserve the reported energy constraints while providing a common temporal resolution for comparing the five system configurations. The reconstructed series should not be interpreted as monitored historical data.

For each load or generation stream x, an unscaled hourly shape factor $w_{x,t}$ was first generated from the available operating descriptors. The final hourly series was then obtained by energy-constrained normalization:

$$P_{x,t} = E_x \frac{w_{x,t}}{\sum_{\tau=1}^{8760} w_{x,\tau}} \quad (1)$$

where $P_{x,t}$ is the reconstructed hourly power in kW, E_x is the reported annual energy in kWh, and the time step is 1 h.

2.2.1. Service Area Demand

The reported annual electricity demand of Zhehai service area is 300.0 MWh. The hourly profile was informed by a component-based assessment of building services and EV charging, with demand peaks at 10:00–12:00 and 16:00–19:00. Assumed monthly multipliers represent higher summer cooling and winter heating and lighting demand. Weekday and weekend factors and a small deterministic day-to-day modulation were also included to avoid unrealistically identical daily curves. The unscaled service area weight is expressed as

$$w_{s,t} = d_{h(t)} \cdot m_{m(t)} \cdot q_{w(t)} \cdot v_{d(t)}, \quad (2)$$

where $d_{h(t)}$ is the hourly share of the daily profile, $m_{m(t)}$ is the monthly multiplier, $q_{w(t)}$ is the weekday/weekend factor, and $v_{d(t)}$ is the deterministic daily modulation. The resulting weights were normalized using Equation (1) to obtain an annual demand of exactly 300.0 MWh. The monthly multipliers range from 0.89 to 1.12, with weekday and weekend factors of 0.97 and 1.08 and a deterministic daily modulation amplitude of 0.035. The complete coefficients and hourly inputs are supplied in the Supplementary Materials and Data S1.

2.2.2. Tunnel Demand

The tunnel demand was reconstructed separately for lighting and ventilation because the two subsystems have different operating patterns. The engineering materials report a weather-corrected annual lighting demand of 713.1 MWh and an annual ventilation demand of 179.5 MWh, giving a combined tunnel demand of 892.6 MWh. Tunnel lighting was represented as a predominantly continuous load with a modest winter increase, whereas ventilation was assigned a higher daytime contribution and a summer multiplier. Small deterministic variations were added to both components, after which each component was normalized to its reported annual energy:

$$P_{tun,t} = E_{light} \cdot \frac{w_{light,t}}{\sum_{\tau=1}^{8760} w_{light,\tau}} + E_{vent} \cdot \frac{w_{vent,t}}{\sum_{\tau=1}^{8760} w_{vent,\tau}} \quad (3)$$

This component-wise treatment preserves both the total tunnel demand and the different operating characteristics of lighting and ventilation. Because no traffic-responsive ventilation measurements were available, short-duration ventilation peaks and incident-related operating modes are outside the scope of the base model.

2.2.3. PV Generation

The PV system has a reported installed capacity of 608 kWp and reported monthly generation of 40, 57, 85, 98, 99, 94, 99, 103, 85, 62, 45, and 37 MWh from January to December, respectively. These monthly values sum to 904 MWh and were used as hard calibration targets. Within each month, the daylight window was estimated from the site latitude and solar declination. A smooth sine-shaped daylight function with an exponent of 1.45 and a deterministic day-to-day modulation factor was used to distribute the monthly energy among daylight hours [43]:

$$P_{\mathrm{PV},t} = E_{\mathrm{PV},m} \cdot \frac{g_t}{\sum_{\tau \in m} g_\tau}, t \in m \quad (4)$$

where g_t is the unscaled daylight-shape factor and $E_{\mathrm{PV},m}$ is the reported PV energy in month m. In addition, to assess dependence on the selected exponent, six values—0.9, 1.00, 1.20, 1.45, 1.70, and 2—were tested with the daylight windows, daily modulation, and monthly generation held unchanged. The calculations were repeated with reconstructed loads and with both external load profiles; the results are reported in Section 3.5.5.

Thus, the annual PV capacity factor is an outcome of the reported energy and installed capacity, while the intraday and day-to-day shapes are reconstructed. Wind generation is not included in the evidence-based base cases because the materials do not provide a project-specific wind turbine configuration or a validated wind generation time series (Figure 3).

2.3. Scenario Definitions and Hourly Dispatch Model

All scenarios use a common system boundary comprising the Zhehai service area and Xiniushan Tunnel. Grid purchases at both nodes are included in every scenario, including cases without an interconnection. Table 1 defines the equipment configurations: S0 is the grid-supplied baseline, S1 includes PV, S2 adds local battery storage, S3 combines PV with an interconnection, and S4 includes all three components. S4 is evaluated using two dispatch priorities, S4-B and S4-T, with identical equipment capacities and costs.

Table 1. Scenario definitions under the common corridor boundary.

Scenario	PV Capacity (kWp)	Battery Capacity (kWh)	Link Input Power Limit (kW)	PV Surplus Priority
S0	—	—	—	Not applicable
S1	608	—	—	Export
S2	608	335	—	Battery charging → export
S3	608	—	500	Tunnel supply → export
S4-B	608	335	500	Battery charging → tunnel supply → export
S4-T	608	335	500	Tunnel supply → battery charging → export

The model operates at hourly intervals ($\Delta t = 1$ h; 8760 intervals per year), with the system architecture and alternative allocation priorities illustrated in Figure 4. PV first meets the simultaneous service area demand. When a deficit remains, the battery, where installed, discharges before grid electricity is purchased. For PV surplus, S4-B prioritizes battery charging before supplying the tunnel, whereas S4-T prioritizes tunnel supply before battery charging. S1 exports the surplus directly; S2 charges the battery before exporting;

and S3 supplies the tunnel before exporting. Residual tunnel demand is supplied by the grid. Battery charging uses only PV surplus, and battery discharge serves only the service area. These fixed rules allow the effect of allocation priority to be compared.

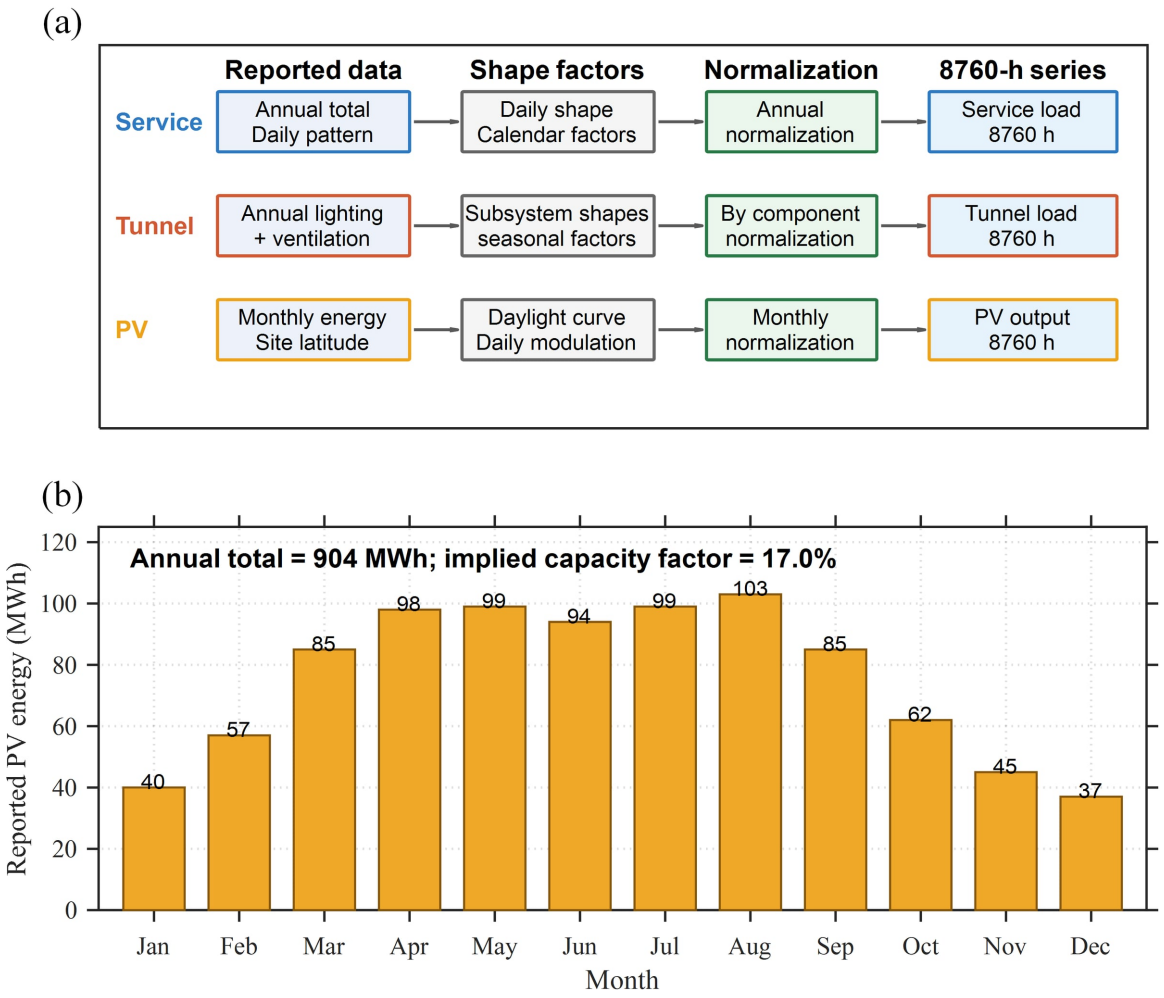


Figure 3. Reconstruction and calibration of representative-year hourly profiles. (**a**) Deterministic reconstruction with exact energy reconciliation. (**b**) Monthly PV values used as hard calibration targets.

For battery capacity C_B in the simulated year, the assumed SOC range is 10–90%, the charge/discharge power limit is 0.5C, and the round-trip efficiency is 90%, with $\eta_{ch} = \eta_{dis} = \sqrt{0.90}$. The 335 kWh reference battery therefore has a 268 kWh storage window and a 167.5 kW power limit. Stored energy is updated as follows:

$$S_{t+1} = S_t + \eta_{ch} E_{ch,t} - \frac{E_{dis,t}}{\eta_{dis}} \tag{5}$$

subject to:

$$0.1C_B \le S_t \le 0.9C_B,\ E_{ch,t} \ge 0,\ E_{dis,t} \le 0.5C_B \tag{6}$$

where S_t is stored energy, C_B is the nominal battery capacity remaining in the simulated year, and $E_{ch,t}$ and $E_{dis,t}$ are the hourly charging and delivered discharging energies. A cyclic annual boundary condition is imposed so that the final SOC equals the initial SOC, preventing the model from creating an artificial year-end benefit.

The service-area/tunnel connection is represented by a 0.65 km equivalent link, corresponding to the midpoint of the reported 0.60–0.70 km distance range. Its efficiency and

transfer limit are assumed to be 97% and 500 kW, respectively. For transferred energy $E_{\mathrm{tr},t}$, the renewable energy received by the tunnel is

$$E_{\mathrm{tun,ren},t} = \eta_{\mathrm{link}} E_{\mathrm{tr},t},\ 0 \le E_{\mathrm{tr},t} \le P_{\mathrm{link,max}} \Delta t. \tag{7}$$

At every hour, the common-boundary energy balance is checked as follows:

$$\begin{aligned} E_{\mathrm{PV},t} + E_{\mathrm{grid},t} = E_{\mathrm{s},t} + E_{\mathrm{tun},t} + E_{\mathrm{exp},t} + E_{\mathrm{curt},t} \\ + E_{\mathrm{link,loss},t} + E_{\mathrm{B,loss},t} + \Delta S_t \end{aligned} \tag{8}$$

$E_{\mathrm{grid},t}$ includes purchases at both nodes, $\Delta S_t = S_{t+1} - S_t$, with $E_{\mathrm{link,loss},t} = (1 - \eta_{\mathrm{link}}) E_{\mathrm{tr},t}$ and $E_{B,\mathrm{loss},t} = (1 - \eta_{\mathrm{ch}}) E_{\mathrm{ch},t} + \left(\eta_{\mathrm{dis}}{}^{-1} - 1\right) E_{\mathrm{dis},t}$. Residual PV is exported, so curtailment is zero in the reference simulations.

For each annual load, PV and battery capacity configuration, the initial stored energy is determined by repeated annual dispatch until $|S_{\mathrm{end}} - S_{\mathrm{start}}| < 10^{-8}$ kWh, with a maximum of 50 iterations. The subsequent annual simulation checks the cyclic boundary, hourly energy balance, SOC bounds and power limits. These checks also apply to the annual dispatch calculations used in the 25-year cash flow analysis.

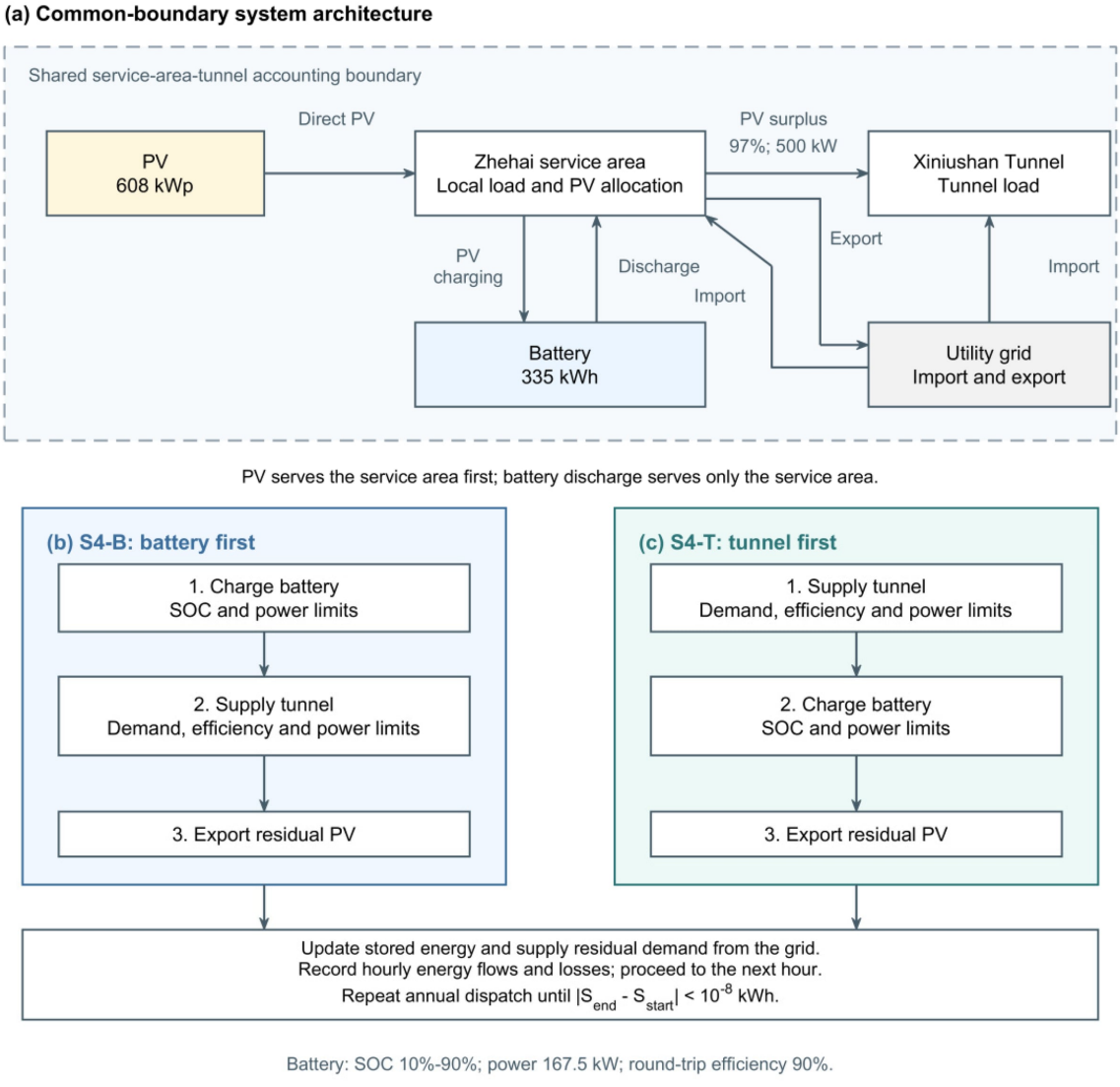


Figure 4. Common-boundary system architecture and alternative hourly dispatch priorities.

2.4. Performance and Economic Evaluation

Technical indicators were calculated from the annual sum of the hourly energy flows. To avoid ambiguity, two different PV utilization indicators were used. PV self-consumption counts PV energy that ultimately serves a load, either directly, after battery discharge, or after transfer to the tunnel:

$$R_{sc} = \frac{E_{PV\to s} + E_{B\to s} + E_{tun,ren}}{E_{PV}} \quad (9)$$

PV absorption is a broader accounting indicator that excludes only exported and curtailed PV energy:

$$R_{abs} = 1 - \frac{E_{exp} + E_{curt}}{E_{PV}} \quad (10)$$

The difference between Equations (9) and (10) consists mainly of battery conversion losses and connection losses. The corridor renewable self-sufficiency ratio is the renewable energy delivered to the two loads divided by their combined demand:

$$R_{corr} = \frac{E_{PV\to s} + E_{B\to s} + E_{tun,ren}}{E_s + E_{tun}} \quad (11)$$

The service area renewable self-sufficiency ratio and tunnel renewable share were also reported separately. Grid purchase reduction was calculated relative to S0 using the same common-boundary load and tariff schedule. Reference peak, flat, and valley purchase prices were set to 0.69, 0.46, and 0.23 CNY/kWh, respectively, using a flat-price baseline of 0.46 CNY/kWh and the 1.5:1:0.5 ratio specified in Yunnan's time-of-use pricing framework. Exported electricity was valued at 0.3358 CNY/kWh, corresponding to the regional coal-fired generation benchmark. The assigned hourly tariff periods are provided in Supplementary Table S10.

Grid-related operational CO_2 emissions were calculated using the electricity emission factor method. The 2023 Yunnan provincial average electricity CO_2 emission factor of 0.1333 kg CO_2/kWh, officially released by the Ministry of Ecology and Environment and the National Bureau of Statistics of China, was adopted as the initial value. The factor was held constant in the reference case. To assess the influence of grid decarbonization, two additional scenarios with annual declines of 2% and 4% were evaluated over the 25-year assessment. The year-dependent factor was defined as $EF_{grid,y} = 0.1333(1-g)^{y-1}$, where $g = 0$, 0.02, 0.04. For scenario i in year y, grid-related operational emissions and avoided emissions relative to S0 were calculated as follows:

$$C_{grid,i,y} = E_{grid,i,y}\, EF_{grid} \quad (12)$$

$$ER_{i,y} = (E_{grid,S0,y} - E_{grid,i,y})\, EF_{grid,y} \quad (13)$$

The cumulative 25-year grid-related CO_2 reduction was calculated as follows:

$$ER_{i,25} = \sum_{y=1}^{25} ER_{i,y} \quad (14)$$

For reporting in kilotonnes, the result was converted using the following:

$$ER_{i,25}{}^{(kt)} = \frac{ER_{i,25}}{10^6} \quad (15)$$

Exported PV electricity was not assigned an additional emissions reduction credit; it contributed only to feed-in revenue in the economic calculation. Therefore, the reported reduction represents avoided grid purchases within the common service-area-plus-tunnel boundary. This conservative treatment prevents the same exported electricity from being

credited both inside and outside the study boundary. The calculation covers operational grid-related CO_2 emissions only and excludes the embodied and end-of-life emissions of PV modules, batteries, and connection infrastructure; it should therefore not be interpreted as a full lifecycle carbon assessment. The primary carbon assessment quantifies operational CO_2 emissions associated with grid electricity purchases. An additional component, emissions screening, uses published PV module and battery pack proxy factors, including the initial battery pack and two replacements over the 25-year period. This screening covers the lifecycle stages represented by the selected factors.

Annual service area demand was set to 300, 601, 1087, 1752, 2235 and 2550 MWh in years 1, 5, 10, 15, 20 and 25, respectively, with log-linear interpolation between these anchors; tunnel demand was held constant. PV output is reduced by 0.5% annually. Battery capacity retention declines linearly by 2% points annually to an 80% floor and resets to 100% upon replacement in years 11 and 21, each costing 70% of the initial battery investment. The 0.5 C power limit follows the remaining capacity.

The annual net benefit is the avoided grid purchase cost plus export revenue, less annual operation and maintenance expenditure. The net present value (NPV) is as follows:

$$\mathrm{NPV} = -I_0 + \sum_{y=1}^{25} \frac{B_y - C_y}{(1+r)^y} \tag{16}$$

where I_0 is the initial investment, B_y is the annual gross benefit, C_y includes operation, maintenance, and replacement expenditure, and r = 8% is the assumed discount rate. The internal rate of return is the rate that makes NPV equal to zero. Simple payback is reported as the first year in which the undiscounted cumulative cash flow becomes non-negative; it is not used as a substitute for NPV.

To isolate the economic contribution of storage, S2 was compared with S1, and S4-B and S4-T were each compared with S3. Incremental cash flows were obtained from $\Delta \mathrm{CF}_y = \mathrm{CF}_{\text{with B},y} - \mathrm{CF}_{\text{without B},y}$, including the initial investment difference. The incremental NPV is as follows:

$$\Delta \mathrm{NPV}_B = \mathrm{NPV}_{\text{with B}} - \mathrm{NPV}_{\text{without B}} \tag{17}$$

Incremental payback was calculated from these cash flow differences. Battery capacities from 1 to 700 kWh were examined, with the battery-free configuration as the reference. Break-even installed cost and purchase price conditions were determined by $\Delta \mathrm{NPV}_B = 0$. Sensitivity cases included discount rates of 4%, 8% and 12%; annual battery fade of 1%, 2% and 3%; purchase price levels of 80%, 100% and 120% of the reference; and annual purchase price changes of −1%, 0% and +1%. Export tariffs, investment, maintenance and replacement costs were also varied. Alternative load profiles were compared at unchanged annual demands. These comparisons assess sensitivity to input assumptions; the ranges are not statistical confidence intervals. The principal technical and economic parameters are shown in Table 2.

2.5. Model Verification and Scope

Verification was performed at the input, hourly balance, state, and financial accounting levels. The generated files contain exactly 8760 hourly records. Annual service area demand, tunnel demand, and PV generation reproduce their reported totals of 300.0, 892.6, and 904.0 MWh, respectively, and each of the 12 monthly PV totals is reproduced exactly. For every scenario and every hour, the residual of Equation (8) is required to be below 10^{-4} kWh. Battery SOC is checked against its upper and lower bounds, and the cyclic year-end condition is enforced. The discounted cash flow indicators are also recalculated independently from the exported annual cash flow tables (Table 3).

Table 2. Principal technical and economic parameters used in model.

Group	Parameter	Value	Group	Parameter	Value
PV	Installed capacity	608 kWp	Tariff	Peak/flat/valley price	0.69/0.46/0.23 CNY/kWh
PV	Annual/monthly generation	904 MWh	Tariff	Export price	0.3358 CNY/kWh
PV	Annual degradation	0.5% $year^{-1}$	Investment	PV; battery	2.240; 0.375 million CNY
Battery	Energy capacity	335 kWh	Investment	Link cable; terminals	0.600 million CNY/km; 0.200 million CNY
Battery	Power limit; SOC range; round-trip efficiency	0.5C; 10–90%; 90%	Economics	Analysis period; discount rate	25 years; 8%
Battery	Capacity fade; minimum capacity	2%/year; 80%	Carbon	Initial grid CO_2 emission factor	0.1333 kg CO_2/kWh
Battery	Replacement years and cost fraction	Years 11 and 21; 70%	Carbon	Emissions credit for exported PV electricity	None
Link	Equivalent distance	0.65 km	Carbon	Component emissions	PV module and battery pack screening
Link	Efficiency; transfer limit	97%; 500 kW			

Table 3. Numerical verification criteria applied before scenario comparison.

Verification Item	Acceptance Criterion	Model Result
Time-series length	8760 hourly records	Passed
Annual service area demand	300.0 MWh	Exact reconciliation
Annual tunnel demand	892.6 MWh	Exact reconciliation
Monthly and annual PV generation	12 reported monthly values; 904.0 MWh/year	Exact reconciliation
Hourly common-boundary balance	Maximum absolute residual $< 10^{-4}$ kWh	Passed; maximum 3.73×10^{-9} kWh
Battery state constraints	SOC within 10–90%; cyclic annual boundary	Passed
Economic calculation	Independent NPV recomputation	Passed; difference $< 10^{-8}$ CNY

These checks establish numerical consistency, but they do not constitute validation against field-monitored 8760 h data. The principal limitation is temporal uncertainty: annual and monthly quantities are reported, whereas coincidence among load, PV generation, and tunnel operation is reconstructed. Accordingly, the analysis is intended for comparative scenario evaluation rather than short-term operational forecasting. Conclusions that depend strongly on battery limits, connection cost, export price, or temporal coincidence should be interpreted together with the sensitivity results. Future monitoring should prioritize synchronized hourly metering at the PV inverter, service area grid connection, battery terminals, and tunnel feeder.

2.6. Comparison with External Load Profiles

To further assess the reliability of findings based on the reconstructed load profiles, this study introduced annual hourly load profiles derived from measurements at an expressway service area and a tunnel in the neighboring province of Guangxi. Calculations were performed using the reconstructed project loads and the external reference loads, while annual electricity demands and other model conditions were held constant. The robustness

of the findings was assessed by examining their sensitivity to changes in the temporal distribution of demand.

For this comparison, the external profiles from Zhang et al. [44] were rescaled to match the case-study annual demands of 300.0 MWh for the service area and 892.6 MWh for the tunnel. A constant factor was applied to all hourly values within each series, preserving the relative hourly distribution and variation between days. Figure 5 displays all 8760 values in each profile as a 365 × 24 heatmap. Loads were divided by their respective annual means, allowing all four panels to share the same color scale.

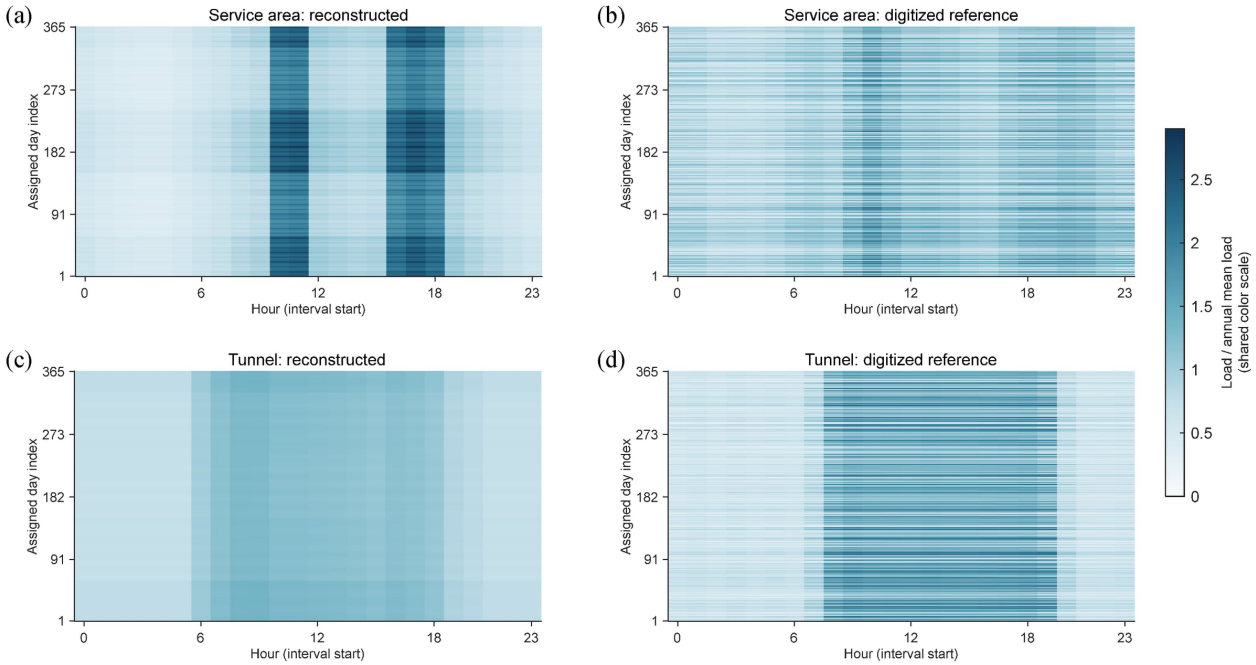


Figure 5. Annual patterns of reconstructed and external load profiles. (**a**) Reconstructed service area demand; (**b**) external digitized service area demand; (**c**) reconstructed tunnel demand; and (**d**) external digitized tunnel demand.

The heatmaps show that both reconstructed and external profiles exhibited higher daytime demand, while differing in peak intensity and daily variability. For the service area (Figure 5a,b), the reconstructed profile displayed two recurring daily peak periods. Its annual peak-to-mean load ratio was 2.86, compared with 2.23 for the external profile. Variation between days was assessed using the coefficient of variation (CV) of daily energy, calculated as its population standard deviation divided by its mean. The CV was 0.116 for the reconstructed profile and 0.341 for the external profile. For the tunnel (Figure 5c,d), both profiles exhibited a sustained daytime load band. The annual peak-to-mean load ratios were 1.40 and 2.34 for the reconstructed and external profiles, respectively. Their daily energy CVs were 0.031 and 0.335. Thus, the external profiles shared the broad daytime loading pattern but included greater variation between days.

These profiles were used to define four input cases: the reconstructed reference, replacement of service area demand only, replacement of tunnel demand only, and replacement of both demands.

3. Results and Discussion

3.1. Lifecycle Economic and Carbon Performance

The energy-constrained reconstruction described in Section 2 produces annual electricity demands of 300.0 MWh for the Zhehai service area and 892.6 MWh for Xiniushan

Tunnel. Their annual mean loads are 34.2 and 101.9 kW, respectively. The tunnel therefore consumes 2.98 times as much electricity as the service area and accounts for 74.8% of the combined 1192.6 MWh corridor demand.

Figure 6a shows the average service area profile in January, April, July, and October. All four curves retain the two operating peaks specified by the project information: a late-morning peak around 10:00–12:00 and a second peak around 16:00–19:00. Seasonal variation changes the magnitude more than the timing of the profile. Across the reconstructed year, the service area load ranges from 12.2 to 98.6 kW. This shape is consistent with a mixed service area demand in which catering, retail, accommodation, and vehicle charging activities are concentrated in recurring operating periods.

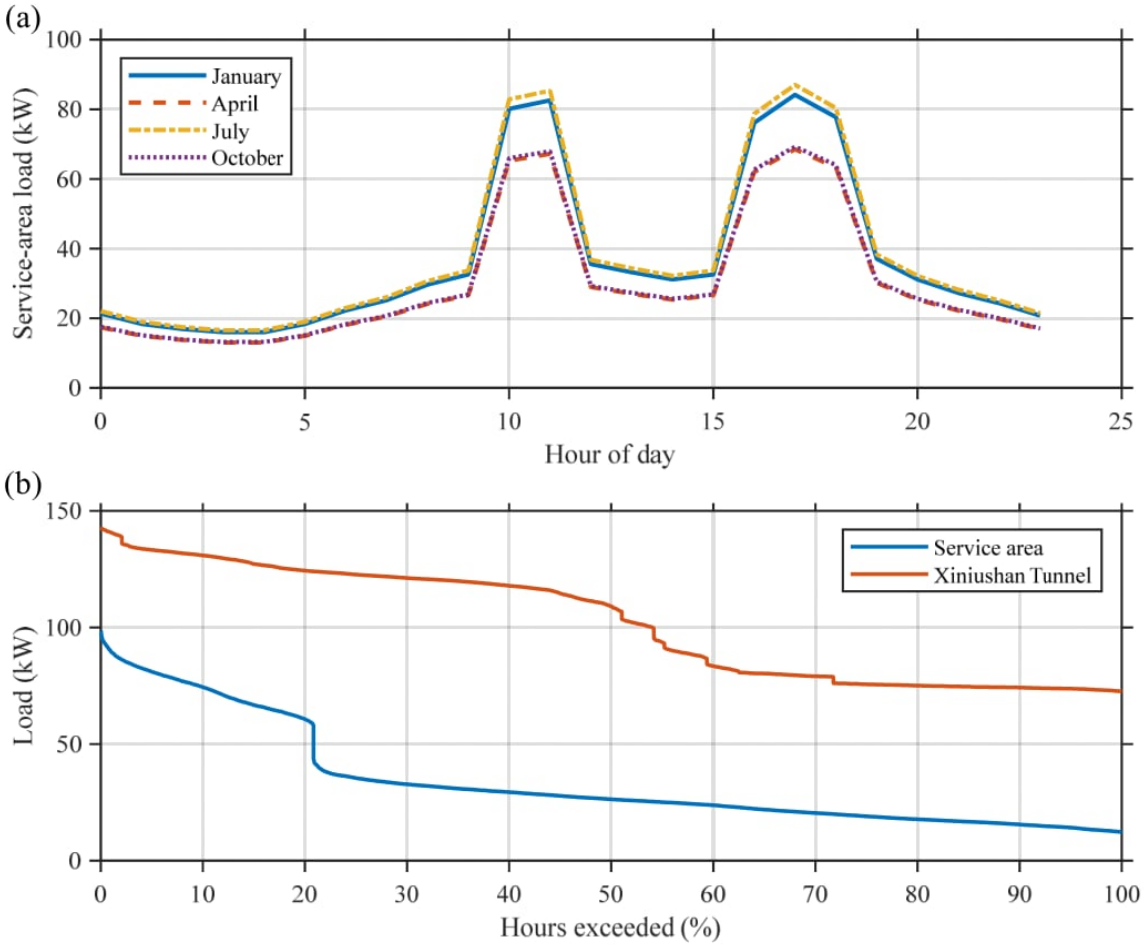


Figure 6. Reconstructed demand characteristics: (**a**) average service area profiles in representative months; and (**b**) annual load–duration curves for service area and Xiniushan Tunnel.

The load–duration curves in Figure 6b show a different operating characteristic at the tunnel node. The reconstructed tunnel load remains between 72.7 and 142.8 kW, whereas the service area curve declines rapidly outside its two daily peaks. The relatively flat tunnel curve arises from continuous lighting, monitoring, safety, and ventilation demand. Consequently, the tunnel is not only the larger consumer but also a stable load anchor. From a system integration perspective, this stability is important because daytime PV surplus that cannot be consumed locally at the service area can potentially be absorbed by the tunnel without introducing a new discretionary load.

These numerical ranges describe a representative-year model constrained by reported energy quantities; they are not field-measured extrema. Their main value is to reveal the contrasting temporal roles of the two nodes before scenario comparison.

3.2. PV Generation and the Chronological Demand Mismatch

The supplied resource information supports a PV-dominated base configuration. The reported representative-year global horizontal irradiation is 1491.81 kWh/m^2, approximately 5.1% below the reported 20-year mean of 1572.04 kWh/m^2. In comparison, the reported wind power density at the service area is only 36.74 W/m^2. Wind generation was therefore excluded from the evidence-based scenarios. This does not rule out locally accelerated wind at tunnel portals, but such a case would require site-specific wind measurements and an identified turbine power curve.

The 608 kWp PV system has a reference annual output of 904.0 MWh, equivalent to 1486.8 kWh/kWp/year. This is 3.01 times the annual service area demand but only 75.8% of the combined service area and tunnel demand. Figure 7 shows that PV generation exceeds service area demand in every month. From March to September, monthly PV generation is 85–103 MWh, while service area consumption is approximately 21.8–28.5 MWh. Thus, the isolated service area has a large annual and monthly energy surplus.

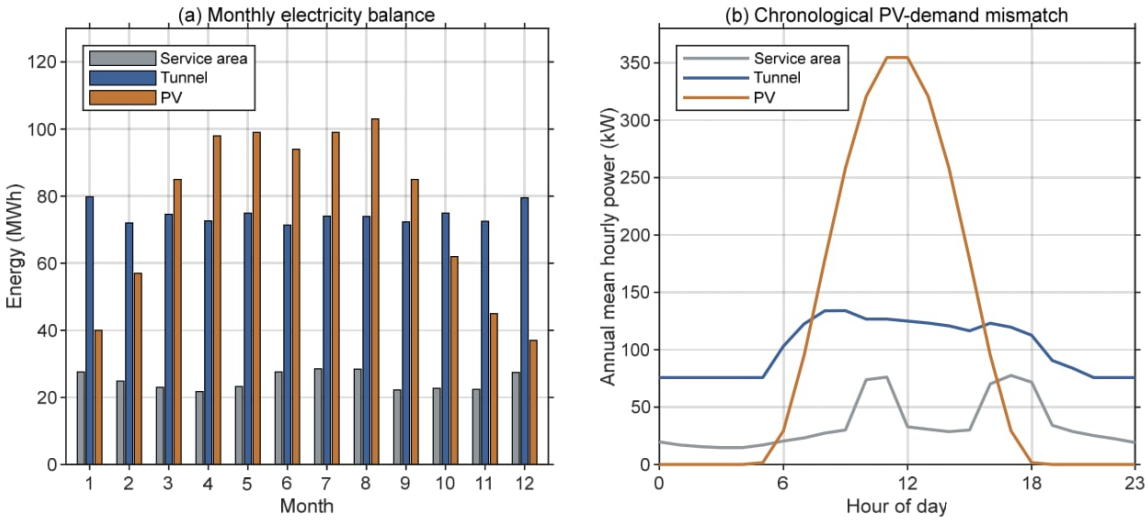


Figure 7. Reconstructed PV generation and electricity demand. (**a**) Monthly energy quantities. (**b**) Annual mean hourly power.

The monthly balance nevertheless overstates the ability of the service area to use PV directly. Generation is concentrated in daylight hours, whereas both nodes continue to consume electricity after sunset. The service area can therefore export PV electricity during the day and purchase electricity during the evening or night within the same month. This chronological mismatch, rather than annual shortage of renewable energy, is the main limitation of the isolated PV configuration.

Figure 7b further illustrates this mismatch through the annual mean hourly profiles. The mean PV output reaches 354.6 kW around 11:00–12:00. At 11:00, the corresponding service area and tunnel loads are 76.2 and 126.7 kW, respectively, leaving 151.7 kW above combined demand. By 17:00, the mean PV output falls to 29.4 kW, while the service area and tunnel require 77.7 and 119.7 kW.

Two integration mechanisms address different parts of the mismatch. Battery storage shifts electricity between hours at the same node, whereas the service area/tunnel link transfers simultaneous surplus to a nearby continuous load. Their relative contributions can therefore be separated by comparing S2 with S1 and S3 with S1.

3.3. Hourly Operation of Storage and Cross-Node Coordination

Figure 8 illustrates the S4-B and S4-T dispatch from 15 to 17 July. This summer window was selected to make the PV surplus management sequence visible; it should not be interpreted as a statistical replacement for the annual results. Both cases use 608 kWp of PV, a 335 kWh battery, the same interconnection, and identical PV and demand inputs (Figure 8a). PV generation first supplies the simultaneous service area demand. In S4-B (Figure 8b), surplus PV then charges the battery until the charging power or upper SOC constraint becomes active. The remaining renewable electricity is transferred to the tunnel, and only the final residual is exported. During service area deficit periods, the battery discharges before grid electricity is purchased. The tunnel purchases the portion of its demand not met by transferred renewable electricity.

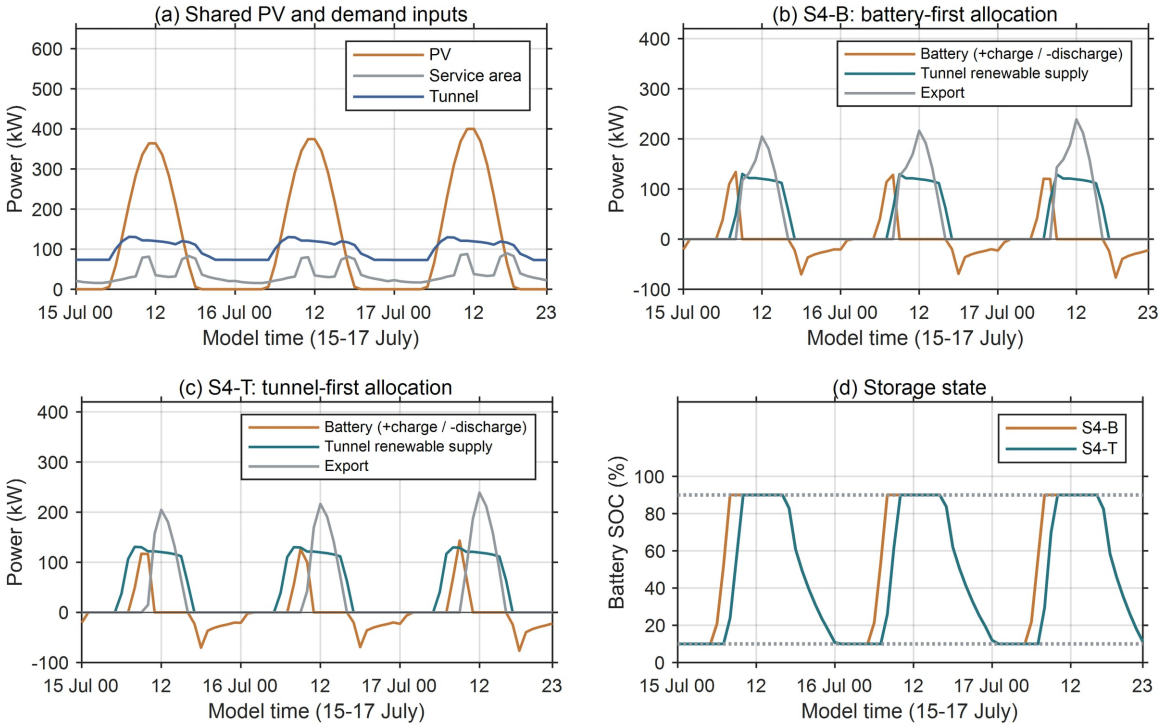


Figure 8. Comparison of S4 dispatch priorities from 15 to 17 July. (**a**) Shared PV generation and electricity demand inputs. (**b**) Battery-first allocation in S4-B. (**c**) Tunnel-first allocation in S4-T. Battery power is positive for charging and negative for discharge. (**d**) Battery SOC trajectories; dotted lines indicate 10% and 90% limits.

The three-day trace demonstrates the physical role of the 335 kWh battery. It charges during the rising part of the PV curve, commonly reaches its upper SOC limit near midday, and discharges after PV generation falls below the service area load. The 10–90% SOC range provides a usable storage window of 268 kWh. However, the battery cannot maintain the service area through the full overnight period. It therefore provides intraday energy shifting rather than multi-day autonomy. Under battery-first dispatch, once the battery is full, the continuous tunnel load becomes the principal internal sink for additional PV generation. Both strategies remain within the specified SOC limits (Figure 8d). The dispatch also exposes an allocation trade-off. The battery-first rule reserves PV surplus for later use at the service area before transferring it to the tunnel. This raises service area self-sufficiency, but it can reduce the tunnel's renewable share. In S4-T (Figure 8c), surplus PV supplies simultaneous tunnel demand before charging the battery. In the illustrated interval, tunnel supply therefore begins earlier and battery charging begins later than in S4-B.

The full-year comparison quantifies the effect of this change in priority. Renewable electricity delivered to the two loads increases from 565.2 MWh in S4-B to 630.7 MWh in S4-T, an increase of 11.59% relative to S4-B. Tunnel renewable supply increases from 306.7 to 386.8 MWh, while service area renewable supply decreases from 258.5 to 243.9 MWh. Battery discharge decreases from 92.8 to 78.2 MWh. The net gain of 65.5 MWh therefore arises from greater simultaneous use of PV surplus, rather than greater battery discharge.

3.4. Technical Contribution of Storage and Cross-Node Coordination

All configurations use the same service-area-plus-tunnel accounting boundary. This prevents a misleading comparison between service area grid purchases in one scenario and total corridor purchases in another. The initial-year results are summarized in Table 4 and Figure 9a.

Table 4. Initial-year technical performance under the common corridor boundary.

Scenario	Useful Renewable (MWh)	Grid Purchases (MWh)	Exports (MWh)	PV Self-Consumption (%)	Corridor Self-Sufficiency (%)	Service Area Self-Sufficiency (%)	Tunnel Renewable Share (%)
S0	0	1192.6	0	—	0	0	0
S1	165.7	1026.9	738.3	18.3	13.9	55.2	0
S2	258.5	934.1	635.2	28.6	21.7	86.2	0
S3	552.6	640	339.5	61.1	46.3	55.2	43.3
S4-B	565.2	627.4	319	62.5	47.4	86.2	34.4
S4-T	630.7	561.9	252.6	69.8	52.9	81.3	43.3

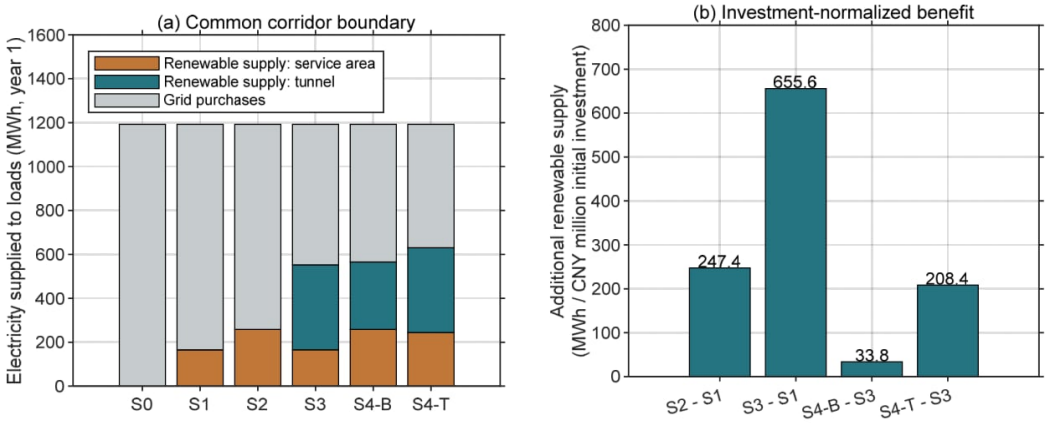


Figure 9. Initial-year technical benefits under a common corridor boundary. (**a**) Electricity delivered to the service area and tunnel loads. (**b**) Additional useful renewable supply per CNY million of additional initial investment, relative to the comparison indicated below each bar.

In S0, the two nodes purchase their full combined demand of 1192.6 MWh from the grid. Adding PV in S1 reduces grid purchases to 1026.9 MWh, but only 165.7 MWh of the 904.0 MWh PV output is delivered to the service area load. The PV self-consumption ratio is therefore 18.3%, while 738.3 MWh is exported. PV supplies 55.2% of annual service area demand, yet the corridor renewable self-sufficiency ratio is only 13.9% because the tunnel remains entirely grid-supplied.

Adding the reported 335 kWh battery in S2 increases renewable electricity delivered to loads by 92.8 MWh relative to S1 and reduces grid purchases by the same quantity. PV self-consumption rises from 18.3% to 28.6%, and service area self-sufficiency rises from 55.2% to 86.2%. Grid export decreases by 103.1 MWh, which exceeds the increase in useful renewable supply because 10.3 MWh is lost in battery conversion. Storage therefore improves local PV

utilization, but its corridor-level effect is limited by the modest service area demand and finite daily cycling capacity.

The spatial coordination effect is substantially larger. In S3, renewable electricity delivered to the tunnel reaches 386.8 MWh after connection losses. Total renewable supply to the two loads rises to 552.6 MWh, PV self-consumption reaches 61.1%, and corridor grid purchases fall to 640.0 MWh. Relative to S1, cross-node coordination adds 386.8 MWh of useful renewable supply, more than four times the 92.8 MWh increment provided by the 335 kWh battery. The stable tunnel demand is therefore the principal source of the integration benefit in this case. Adding storage to S3 further improves aggregate technical performance, but its contribution depends on dispatch priority. In S4-B, renewable electricity delivered to loads reaches 565.2 MWh, grid purchases decrease to 627.4 MWh, and corridor renewable self-sufficiency reaches 47.4%. However, the incremental gain over S3 is small: the battery adds only 12.7 MWh of useful renewable supply and reduces exports by 20.5 MWh after the link is already available. Moreover, the battery-first priority increases service area self-sufficiency to 86.2% but reduces the tunnel renewable share from 43.3% in S3 to 34.4% in S4-B.

S4-T provides the highest corridor renewable self-sufficiency among the tested configurations. Useful renewable supply reaches 630.7 MWh, grid purchases decrease to 561.9 MWh, and PV self-consumption and corridor self-sufficiency reach 69.8% and 52.9%, respectively. Relative to S3, storage adds 78.2 MWh of useful supply under this priority. The tunnel renewable share remains at 43.3%, while service area self-sufficiency reaches 81.3%.

PV absorption is slightly higher than PV self-consumption in S2, S3 and both S4 variants because absorption excludes only exported and curtailed PV, whereas self-consumption counts energy delivered to loads and therefore excludes battery and connection losses. This distinction prevents conversion losses from being misreported as useful renewable supply.

To compare the technical contributions on a consistent investment basis, the initial-year increase in useful renewable supply is divided by additional initial investment:

$$U_{\mathrm{I}} = \frac{\Delta E_{\mathrm{ren}}}{\Delta I_0 / 10^6} \tag{18}$$

Here, ΔE_{ren} is the additional renewable electricity delivered to loads in MWh, and ΔI_0 is the additional initial investment in CNY. Thus, U_{I} is expressed in MWh per CNY million of additional initial investment. S2 relative to S1 provides 247.4 MWh/CNY million, compared with 655.6 MWh/CNY million for S3 relative to S1 (Figure 9b). The interconnection advantage therefore persists after accounting for investment scale. For storage added to S3, the corresponding values are 33.8 MWh/CNY million under battery-first dispatch and 208.4 MWh/CNY million under tunnel-first dispatch.

Table 5 reports annualized incremental equipment costs divided by annualized additional grid electricity displacement. Both costs and avoided grid electricity are discounted over 25 years at 8% and converted to equivalent annual values using the same capital recovery factor (Supplementary Section S5). Electricity savings and foregone export revenue are excluded from this ratio and accounted for in the NPV.

Table 5. Technical benefits and costs normalized to additional component investment.

Comparison	Initial Investment (10^3 CNY)	Year 1 Useful Increment (MWh)	Useful Increment/ Investment (MWh/CNY million)	Annualized Equipment Cost (10^3 CNY/year)	Cost/Annualized Additional Grid Displacement (CNY/kWh)
S2 − S1	375	92.8	247.4	65.6	0.809
S3 − S1	590	386.8	655.6	61.2	0.233
S4-B − S3	375	12.7	33.8	65.6	9.323
S4-T − S3	375	78.2	208.4	65.6	1.288

The scenario ranking depends on the decision objective. S2 and S4-B achieve the highest service area self-sufficiency, whereas S4-T achieves the highest corridor renewable self-sufficiency. S3 captures most of the corridor-wide renewable utilization benefit with less equipment and supplies a larger renewable share to the tunnel than S4-B. S2 is useful when cross-node construction is infeasible, but it cannot exploit the tunnel as a stable renewable sink.

3.5. Economic Performance and Sensitivity

3.5.1. Lifecycle Economic and Carbon Performance

The economic analysis compared savings on grid purchases and PV export revenue with investment, maintenance and replacement costs over 25 years. The assumptions are given in Section 2.4 and Table 2, with complete annual cash flows provided in Supplementary Data S2.

S1 achieved the highest NPV of CNY 1.013 million, an IRR of 12.95% and a simple payback of 8 years. S2 and S3 also had positive NPVs at the reference 8% discount rate, reaching CNY 0.429 and 0.445 million, respectively. However, S3 exceeded S2 by only 3.56% of the magnitude of S2's NPV (Table 6 and Figure 10a). The much larger renewable utilization gain of S3 therefore translated into only a small financial advantage. Internal PV use reduced grid purchases, but the savings had to cover additional equipment costs and the export revenue forgone. S1 avoided these additional costs while continuing to earn revenue from surplus electricity.

Table 6. Whole-system economics over 25 years under the reference assumptions.

Scenario	Investment (CNY million)	NPV (CNY million)	IRR (%)	Simple Payback (year)	Discounted Payback (year)
S1	2.24	1.013	12.95	8	12
S2	2.615	0.429	9.96	9	17
S3	2.83	0.445	9.83	10	18
S4-B	3.205	−0.268	6.96	12	—
S4-T	3.205	−0.165	7.35	12	—

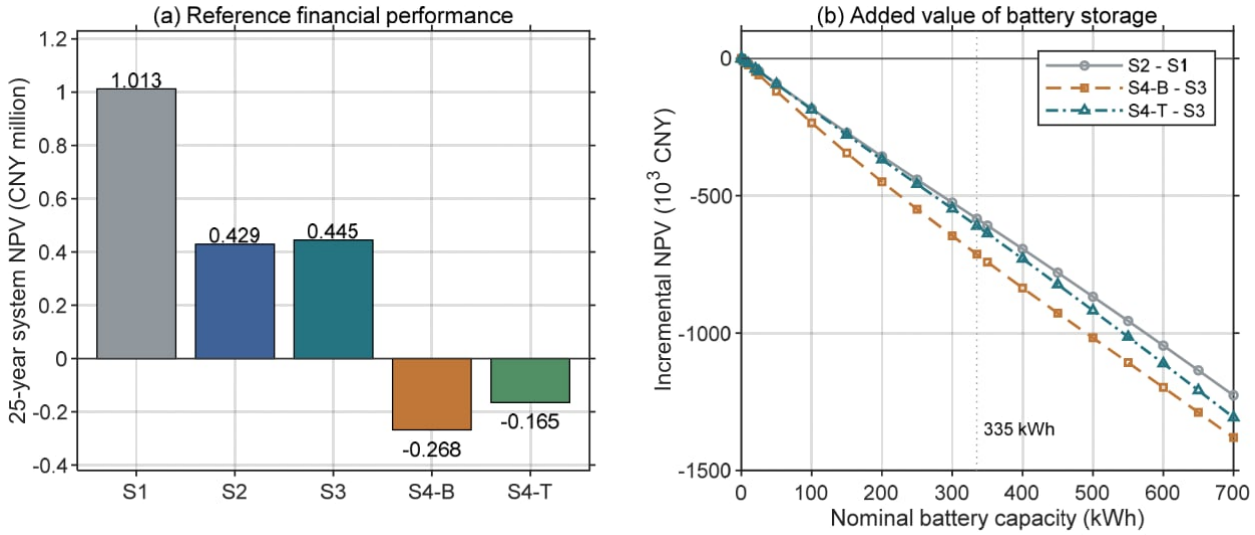


Figure 10. Reference economic performance. (**a**) Whole-system NPV over 25 years. (**b**) Incremental NPV of storage relative to corresponding battery-free configuration; zero capacity is comparison baseline.

The combined configurations required the greatest investment, and their additional electricity savings were insufficient to recover this expenditure at the reference discount rate. S4-B and S4-T had NPVs of CNY −0.268 and −0.165 million, respectively. Giving tunnel supply priority improved the NPV by CNY 102,862 without changing the installed equipment. This improvement followed the greater direct use of PV surplus described in Section 3.3. Both configurations had a simple payback of 12 years, but neither achieved discounted payback within 25 years. Simple payback uses undiscounted cash flows, whereas NPV also accounts for the timing of revenues and replacement expenditure.

Grid decarbonization reduced the operational emissions avoided by all PV configurations (Figure 11a). With the grid emissions factor fixed at 0.1333 kg CO_2/kWh, S3 avoided 2460.3 t CO_2 over 25 years. This decreased to 1921.7 and 1524.7 t when the factor declined by 2% and 4% annually. The same effect reduced the additional savings from storage. Relative to S3, S4-B reduction fell from 19.47 to 13.86 t, the S4-T reduction fell from 126.84 to 96.33 t. As grid electricity becomes less carbon-intensive, a given reduction in grid purchases produces a smaller emissions benefit.

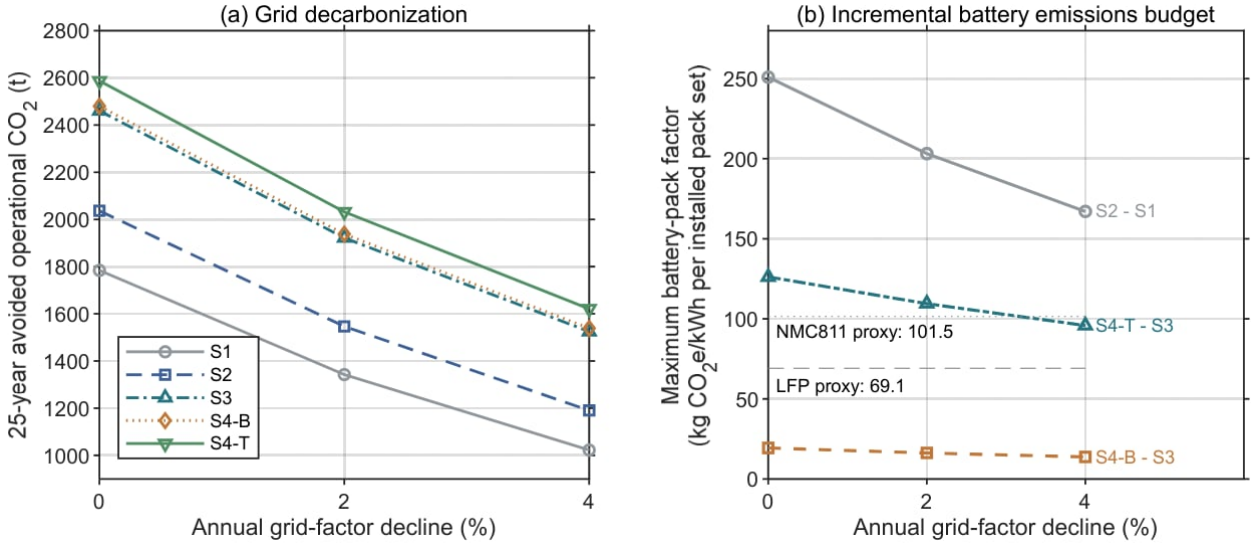


Figure 11. Carbon sensitivity over 25 years. (**a**) Avoided operational CO_2 under grid decarbonization. (**b**) Maximum pack emissions factor for non-negative incremental balance before uncovered storage processes. Three pack sets are counted; horizontal lines mark LFP and NMC811 proxies.

Component emissions can offset some of these operational carbon savings. Using the factors in Supplementary Tables S13 and S14, the PV module estimate was 250.88 t CO_2e. For the 335 kWh LFP battery, the initial pack and two replacements together contributed 69.45 t CO_2e. This exceeded the additional operational savings of S4-B over S3. For S4-T, the NMC811 pack estimate of 102.01 t also exceeded its 96.33 t operational increment under 4% annual grid decarbonization (Figure 11b). The common PV and interconnection components cancel in these S4–S3 comparisons, leaving storage as the additional emissions source. A complete lifecycle balance would also require emissions from other storage equipment, transport, installation and end-of-life processes.

3.5.2. Battery Capacity Sensitivity

Battery capacity was varied to determine whether a different size could improve the return on storage investment. Twenty positive capacities between 1 and 700 kWh were compared, with investment, maintenance and replacement costs scaled to nominal capacity. Returns from adding storage were calculated relative to the corresponding configuration without a battery, using S1 for S2 and S3 for both S4 variants. At 335 kWh, incremental

NPVs were CNY −0.583 million for S2, −0.713 million for S4-B and −0.610 million for S4-T (Figure 10b). None of the tested positive capacities recovered the additional investment within 25 years.

The negative incremental NPV persisted across 1620 combinations of capacity, dispatch rule, purchase price, discount rate and battery degradation. Maintenance costs were particularly restrictive. At 45 CNY/kWh/year, the 335 kWh battery remained unprofitable even when its initial investment was set to zero. Reducing maintenance to 15 CNY/kWh/year increased the S2 break-even installed cost to 132.2 CNY/kWh. At an illustrative installed cost of 100 CNY/kWh and a maintenance cost of 15 CNY/kWh/year, the 335 kWh S2 battery achieved a positive incremental NPV of CNY 15,538 over 25 years at an 8% discount rate. This example illustrates how lower investment and maintenance costs can support storage investment under the NPV criterion.

3.5.3. Component Capacity and Connection Cost Sensitivity

PV capacity determined the surplus available for tunnel demand, affecting the financial comparison between S2 and S3. Increasing capacity from 400 to 800 kWp raised S3's useful renewable supply from 479.9 to 588.0 MWh (Supplementary Table S1). Its NPV increased from CNY 0.071 to 0.764 million under proportional PV investment and maintenance costs. The useful PV fraction nevertheless fell from 80.7% to 49.4%, because coincident demand could absorb a smaller proportion of the larger PV output. At 400 and 500 kWp, S2 had a slightly higher NPV than S3. With less surplus available, the savings from tunnel supply were less able to offset the fixed cost of interconnection.

The 500 kW transfer limit did not restrict operation in the tested cases. Peak first-year transfer input was 147.2 kW with reconstructed demand and 244.0 kW with the external tunnel profile. Limits of 250, 500 and 1000 kW produced identical economic results for the reconstructed and dual-profile external demand cases. This establishes the adequacy of 500 kW for the tested inputs, although an economic optimum requires connection costs to vary with the rating.

The cost of constructing the connection was more consequential for the comparison between S2 and S3. With annual link maintenance at 1% of investment, S3 matched S2 at a link investment of approximately CNY 0.604 million. This was only 2.34% above the CNY 0.590 million reference. A relatively small construction cost increase could therefore remove the financial advantage of S3.

3.5.4. Sensitivity to Alternative Load Profiles

The Guangxi reference profiles were used to examine how the results depended on the hourly distribution of demand. They were scaled to annual consumption of 300.0 MWh for the service area and 892.6 MWh for the tunnel. The service area profile, tunnel profile and both profiles were replaced in turn, while PV generation and other model inputs remained unchanged. Scaling kept this timing comparison independent of differences in annual consumption.

S3 provided an additional 386.8–412.9 MWh of useful renewable electricity relative to S1 across the four cases, compared with 92.3–92.8 MWh for S2 (Figure 12a). Interconnection retained its energy utilization advantage because the tunnel continued to absorb substantial daytime surplus. The financial comparison was more sensitive to the substitutions (Figure 12b), with the absolute NPVs given in Supplementary Table S2. The S3–S2 NPV gap changed from +3.56% to −3.08%, −2.99% and −10.21% when the service area, tunnel and both profiles were replaced, respectively. Each percentage uses the magnitude of S2's NPV in the corresponding case as its denominator. Load timing changes the value

of avoided purchases under hourly tariffs, so the slight reference financial advantage of S3 did not persist across the external profiles.

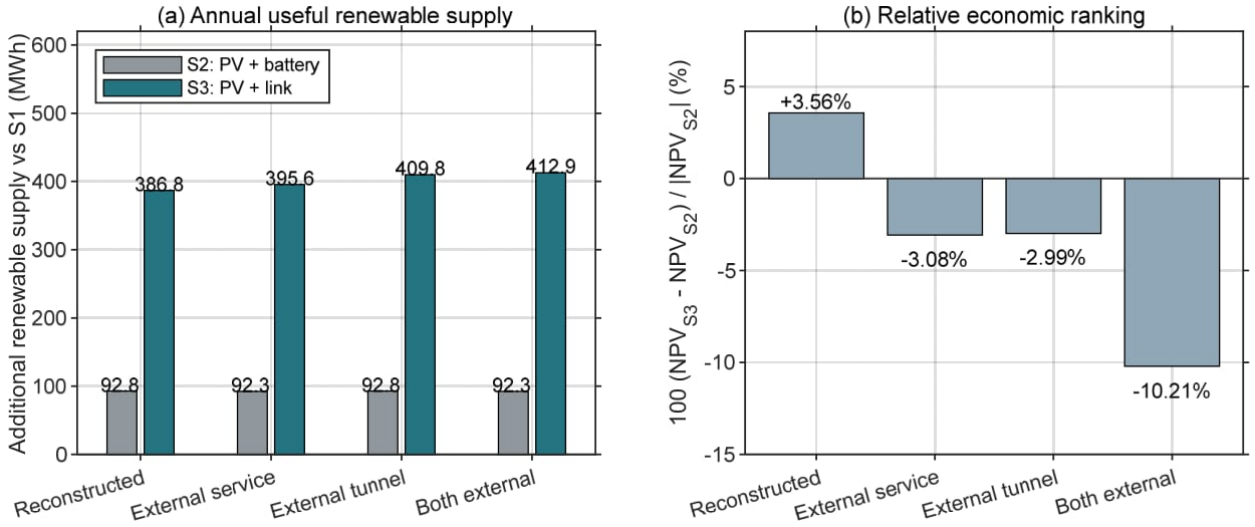


Figure 12. External-load sensitivity at equal annual demands. (**a**) Additional first-year renewable supply relative to S1. (**b**) S3–S2 NPV difference as percentage of magnitude of S2 NPV in same case.

3.5.5. Economic Conditions and Input Uncertainty

Storage also remained unprofitable when purchase prices and discount rates were varied together. For the 335 kWh S2 battery with 2% annual capacity fade, the incremental NPV ranged from CNY −0.869 to −0.428 million (Figure 13a). Higher purchase prices increased the savings from battery discharge, but they did not offset the additional costs within the tested range. Lower discount rates did not improve the incremental NPV because maintenance and replacement expenditure also received greater weight. The maintenance sensitivity in Figure 13b quantifies the cost thresholds discussed above.

Eight cases examined annual PV output ±10%, seasonal weighting modulated by 15%, service area demand shifted by ±2 h and annual demands scaled by ±20% (Figure 13c). Seasonal PV profiles were rescaled to preserve annual generation. Relative to its reference NPV magnitude, S3's NPV changed by −78.7% and +78.2% under annual PV output −10% and +10%, respectively. Annual output affected the total electricity available for internal supply and export, whereas seasonal redistribution mainly changed when that electricity was available. The seasonal cases consequently produced much smaller NPV changes, within 0.8% for both S2 and S3. Shifting service area demand by −2 h and +2 h reduced S3's NPV by 7.0% and 27.5%, respectively, showing the importance of demand timing.

PV intraday shape was additionally examined using six power-sine exponents between 0.9 and 2.0 while preserving each monthly generation total. Across the twelve combinations of exponent and load background, S3 increased first-year renewable electricity delivered to loads by 360.9–441.3 MWh relative to S1, compared with 91.9–92.8 MWh for S2. The utilization advantage of interconnection therefore persisted across the tested shapes. Under reconstructed loads, the relative S3–S2 NPV difference ranged from −0.68% to +8.57%, compared with +3.56% at the reference exponent of 1.45. Each percentage uses the magnitude of S2's NPV in the corresponding case as its denominator. The results support the utilization comparison while identifying PV intraday allocation as a further condition affecting the economic ranking.

Two further cases combined changes in discount rate, purchase price escalation, export tariff, replacement cost and PV degradation over the operating life (Supplementary Table S3). All five PV configurations had negative NPVs under the high-discount/lower-price case

and positive NPVs under the low-discount/higher-price case. However, adding storage to S3 under the S4-T rule still reduced the NPV by CNY 0.506 and 0.771 million, respectively. Even under the favorable case, overall profitability did not make the additional storage investment profitable. These deterministic cases assess dependence on assumed conditions without assigning probabilities to financial outcomes.

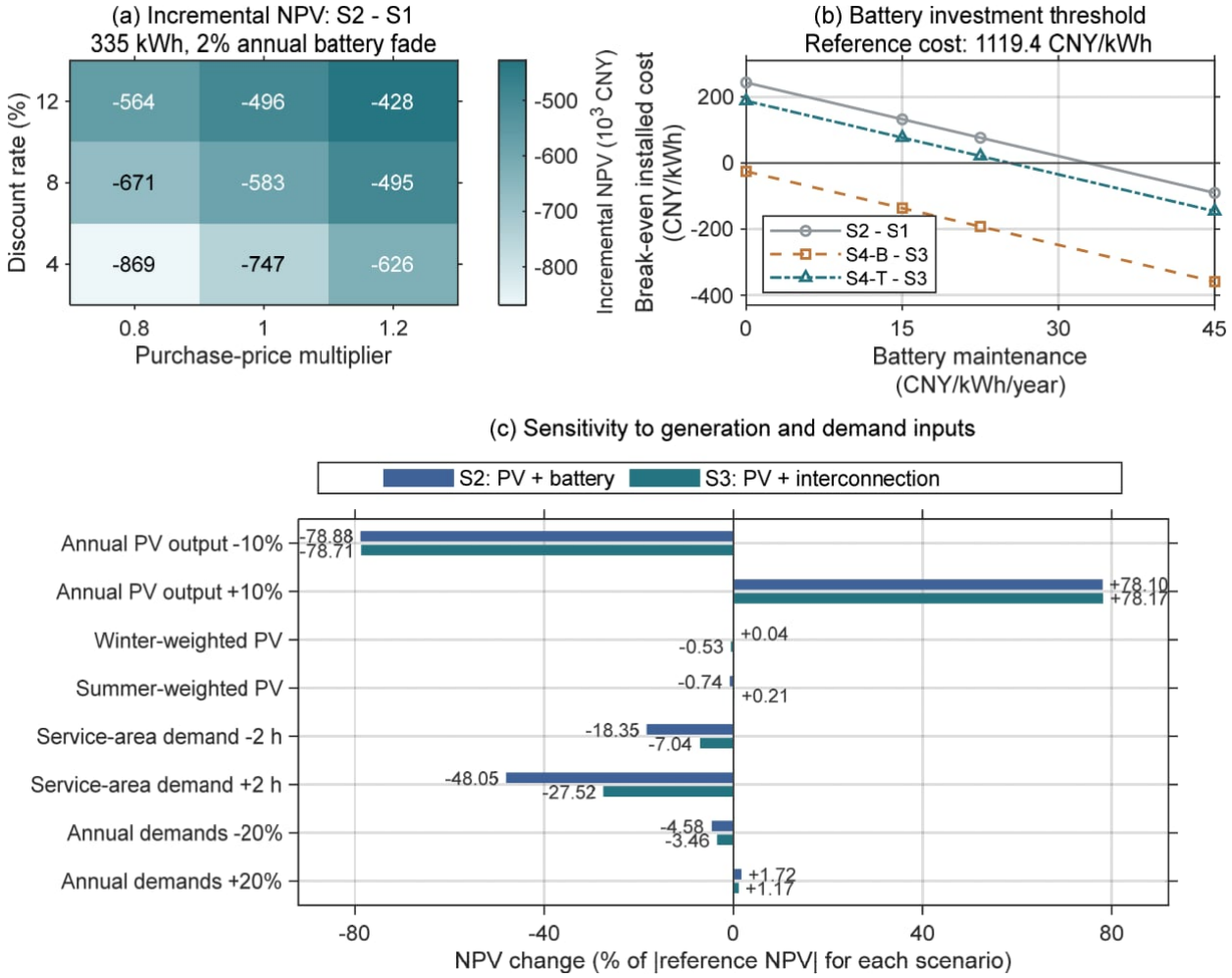


Figure 13. Economic conditions and sensitivity to generation and demand. (**a**) S2–S1 incremental NPV for 335 kWh battery. (**b**) Break-even installed cost versus annual maintenance. (**c**) NPV changes for eight deterministic input cases.

3.6. Practical Implications and Limitations

The comparison supports a staged approach to corridor energy integration. Under the reference assumptions, S1 provided the strongest financial return, while S3 produced substantially greater useful renewable supply than S2. The external-load comparisons retained this utilization advantage but reversed the small S3–S2 NPV advantage. Interconnection should therefore be assessed where coincident tunnel demand and acceptable connection costs justify the investment. Storage requires a separate incremental evaluation, since none of the tested nonzero battery capacities recovered its additional investment under the reference costs. Lower battery and maintenance costs can change this assessment.

Two site ratios help interpret the results: annual PV generation/service area demand was 3.01, and tunnel/service area demand was 2.98. Neither ratio captures hourly coinci-

dence. A complementary transferable indicator is the fraction of service area PV surplus that a tunnel could receive before battery charging:

$$M_{\mathrm{T}} = \frac{\sum_{t=1}^{8760} \eta_{\mathrm{link}} \min\left(P_{\mathrm{sur},t}, P_{\mathrm{link,max}}, \frac{P_{\mathrm{tun},t}}{\eta_{\mathrm{link}}} \right) \Delta t}{\sum_{t=1}^{8760} P_{\mathrm{sur},t} \Delta t} \tag{19}$$

Here, $P_{\mathrm{sur},t}$ is positive service area PV surplus, $P_{\mathrm{tun},t}$ is tunnel demand, $P_{\mathrm{link,max}}$ is the link input limit, η_{link} is link efficiency, and Δt is the hourly interval. The indicator includes transfer losses. It was 0.524 for the reconstructed reference and 0.521–0.555 across the external substitutions. This combination of substantial surplus and coincident tunnel demand explains the consistent energy utilization advantage. The battery usable window, 268 kWh, was only 13.25% of mean daily service area PV surplus, limiting the amount that could be shifted between hours.

Connection cost provides a second screening criterion. Holding dispatch and the link maintenance fraction constant, the investment at which S3 matches S2 in NPV is as follows:

$$I_{\mathrm{link}}{}^{*} = I_{\mathrm{link,ref}} + \frac{\mathrm{NPV}_{\mathrm{S3,ref}} - \mathrm{NPV}_{\mathrm{S2,ref}}}{1 + f_{\mathrm{OM}} \sum_{y=1}^{25} (1+r)^{-y}} \tag{20}$$

Here, $I_{\mathrm{link,ref}}$ is the reference link investment, f_{OM} is its annual maintenance fraction, and r is the discount rate. With a reference investment of CNY 590,000 and 1% annual maintenance, the threshold was CNY 603,824, only 2.34% higher. At the assumed 600,000 CNY/km route cost and CNY 200,000 terminal cost, this corresponds to approximately 0.673 km. This conversion assumes unchanged dispatch and link losses. Actual cable routing, voltage, transformers, protection and right-of-way requirements must be established before construction.

The external reference loads strengthen the temporal sensitivity assessment, but synchronized project measurements are still needed to verify actual PV–load coincidence. Annual and seasonal perturbations do not represent site-specific weather, traffic-responsive tunnel controls or incident operation. Likewise, the fixed dispatch rules do not establish a cost-optimal controller, and the component emissions estimates do not establish a complete lifecycle carbon balance. These uncertainties should be addressed with synchronized monitoring, operational records and equipment inventories before applying the numerical thresholds to another project.

Future work will incorporate traffic-responsive ventilation, adaptive lighting, seasonal traffic variation, incident operation and temporary shutdowns using traffic and tunnel operation records. These analyses will quantify how changes in coincident tunnel demand affect renewable-= electricity transfer and the comparative performance of interconnection and battery storage. Optimization-based control incorporating electricity costs, grid purchases at both nodes and battery cycling degradation will also be investigated.

4. Conclusions

This study compared battery storage and service area–tunnel interconnection for the Zhehai service area and Xiniushan Tunnel using an hourly model and a common corridor boundary. Reconstructed project profiles, external reference loads and sensitivity analyses were used to assess technical, economic and carbon performance. The main conclusions are as follows.

(1) Annual or monthly energy balances cannot substitute for chronological source–load matching. The 608 kWp PV system had a reference annual output of 904.0 MWh, compared with 300.0 MWh of service area demand. However, S1 used only 18.3% of PV generation locally. Temporal mismatch was therefore the main limitation on utilization.

(2) Battery storage and interconnection address different parts of this mismatch, with spatial coordination providing the larger benefit in this case. Relative to S1, S2 added 92.8 MWh of useful renewable supply in the first year, whereas S3 added 386.8 MWh after connection losses. In the combined configuration, tunnel-first dispatch increased useful supply from 565.2 to 630.7 MWh, 11.59% above battery-first dispatch, and achieved 52.9% corridor self-sufficiency.

(3) The configuration with the highest corridor renewable supply did not provide the greatest financial return. Over 25 years, S1 achieved the highest NPV of CNY 1.013 million, whereas S4-T remained negative at CNY −0.165 million. None of the tested nonzero battery capacities between 1 and 700 kWh recovered its incremental investment under the reference costs. Lower investment and maintenance costs can change this result, so storage requires a separate assessment of its additional costs and savings.

(4) The utilization advantage of interconnection persisted when the Guangxi reference load profiles were substituted at equal annual demands. Across the reference and substituted cases, S3 added 386.8–412.9 MWh of useful renewable supply relative to S1, compared with 92.3–92.8 MWh for S2. However, the S3–S2 NPV gap changed from +3.56% to between −10.21% and −2.99%, using the magnitude of S2's NPV in each case as the denominator. Economic ranking was therefore more sensitive to load timing than renewable utilization.

(5) Grid decarbonization reduced the operational carbon benefit of PV and storage. For S3, 25-year avoided emissions fell from 2460.3 t CO_2 with a constant grid factor to 1524.7 t under a 4% annual decline. Battery production and replacement could offset the small additional operational savings of storage. These estimates support carbon screening but do not represent a complete lifecycle assessment.

These results support a staged approach in which PV is assessed first, interconnection is evaluated against coincident tunnel demand and connection cost, and storage is justified separately. Synchronized project monitoring and detailed connection design remain necessary before investment decisions, because external load comparisons do not verify site-specific PV generation or operating conditions.

Supplementary Materials: The following supporting information can be downloaded at https://www.mdpi.com/article/10.3390/en19215342/s1. Table S1. PV-capacity sensitivity with proportional PV investment and maintenance. Table S2. External-load economic comparison at equal annual demands. Table S3. Joint economic cases with five parameters varied simultaneously. Table S4. Sensitivity to the PV power-sine exponent. Table S5. Hourly weights before annual normalization. Table S6. Monthly PV quantities and load multipliers. Table S7. Calendar factors and deterministic modulation. Table S8. Principal reference technical and economic parameters. Table S9. Service-area annual demand anchors. Table S10. Reference hourly purchase and export prices. Table S11. Investment-normalized and annualized comparison. Table S12. Reference operational CO_2 sensitivity over 25 years. Table S13. PV-module EPD proxy factors per Wp. Table S14. Battery-pack chemistry proxies used in the main screening. Table S15. Break-even pack factor before uncovered storage processes. Table S16. Battery-capacity sensitivity of incremental NPV. Table S17. Break-even installed battery cost at 335 kWh. Table S18. Reference annual net cash flows including year 0.

Author Contributions: Conceptualization, G.S.; methodology, D.D. and Y.T.; software, Y.W.; validation, D.D., Y.W. and A.W.; formal analysis, A.W. and Q.Q.; investigation, D.D., H.S. and Q.Q.; resources, Q.Q.; data curation, H.S. and Y.X.; writing—original draft preparation, D.D.; writing—review and editing, G.S., Y.X. and Q.Q.; visualization, Y.W. and A.W.; supervision, Q.Q. and Y.T.; project administration, Q.Q. and Y.T.; funding acquisition, Q.Q. and Y.T. All authors have read and agreed to the published version of the manuscript.

Funding: This research was funded by Science and Technology Innovation Project of Department of Transport of Yunnan Province (Grant number: YJKJB [2023]153).

Data Availability Statement: The original contributions presented in this study are included in thearticle. Further inquiries can be directed to the corresponding author.

Conflicts of Interest: Authors Dajian Dong, Yongxing Wang, Yue Tong and Anping Wang were employed by the Yunnan Xuanhui Expressway Co, LTD. The remaining authors declare that the research was conducted in the absence of any commercial or financial relationships that could be construed as a potential conflict of interest.

References

1. Yao, L.; Fu, H.; Shao, M.; Yu, Z. Highway Microgrid Project Evaluation under Energy Transportation Integration. *Appl. Sci.* **2024**, *14*, 2707. [CrossRef]
2. Zhang, Y.X.; Yin, Z.L.; Xiao, H.G.; Luo, F.J. Coordinated Planning of EV Charging Stations and Mobile Energy Storage Vehicles in Highways With Traffic Flow Modeling. *IEEE Trans. Intell. Transp.* **2024**, *25*, 21572–21584. [CrossRef]
3. Peerlings, J.; Reinders, A.; Catita, C.; Brito, M.C. The photovoltaic potential for electric vehicle charging along highways: A Dutch case study. *Prog. Photovolt.* **2024**, *32*, 244–252. [CrossRef]
4. Kim, S.; Lee, Y.; Moon, H.R. Siting criteria and feasibility analysis for PV power generation projects using road facilities. *Renew. Sustain. Energy Rev.* **2018**, *81*, 3061–3069. [CrossRef]
5. Shi, Z.; Wu, H.; Xiao, T.; Huang, X.; Shao, L.; Ma, Z.; Cao, P. Planning and Energy Self-Supply Strategy for Distributed Photovoltaic Microgrids on Highways Considering Regional Layout Constraints. *Processes* **2025**, *13*, 1377. [CrossRef]
6. Shi, R.; Gao, Y.; Zhang, J.; Jia, L.; Lee, K.Y. A planning method for energy storage capacity of highway self-consistent multi-microgrid system considering carbon trading. *J. Energy Storage* **2024**, *100*, 113616. [CrossRef]
7. Zhang, S.; Jiang, W.; Wang, T.; Zhang, Y.; Yuan, D. A Comprehensive Framework for the Design and Evaluation of Photovoltaic Self-Sufficient Energy Systems in Highway Service Areas. *Renew. Energy* **2026**, *256*, 123877. [CrossRef]
8. Bracale, A.; Caramia, P.; Varilone, P.; Verde, P. Probabilistic Estimation of the Energy Consumption and Performance of the Lighting Systems of Road Tunnels for Investment Decision Makin. *Energies* **2019**, *12*, 1488. [CrossRef]
9. Zhu, S.; Xue, Z.; Li, Y.; Xu, C.; Ma, S.; Li, Z.; Lin, F. Robust Scheduling of Multi-Service-Area PV-ESS-Charging Systems Along a Highway Under Uncertainty. *Energies* **2026**, *19*, 372. [CrossRef]
10. Xu, J.; Liu, Z.; Jiang, H. Study on Application of Solar Energy in Highway. *E3S Web Conf.* **2021**, *261*, 01060. [CrossRef]
11. Xu, X.; Wu, J.; Lu, Y.; Liu, Y.; Zhao, H. A spatio-temporal prediction approach for charging load of clustered electric vehicles in dynamic traffic flow environment of highway. *Sustain. Energy Grids Netw.* **2024**, *40*, 101593. [CrossRef]
12. Zhao, J.D.; Feng, Y.Z.; Yang, C. Intelligent control and energy saving evaluation of highway tunnel lighting: Based on three-dimensional simulation and long short-term memory optimization algorithm. *Tunn. Undergr. Space Technol.* **2021**, *109*, 103768.
13. Lin, X.H.; Yan, Z.G.; Shen, Y.; Guo, C.; Hu, L.F. Combined ventilation mode in extra-long road tunnels: Energy efficient channel utilization with the inclined shafts. *Build. Environ.* **2025**, *269*, 112342. [CrossRef]
14. Wang, Y.M.; Zhou, C.X.; Zhao, Q.T.; Jia, R.H.; Wu, W. Ventilation control of road tunnels towards disturbance suppression. *Sci. Rep.* **2024**, *14*, 2307. [CrossRef] [PubMed]
15. Ahmad, S.; Mujeebu, M.A.; Farooqi, M.A. Energy harvesting from pavements and roadways: A comprehensive review of technologies, materials, and challenges. *Int. J. Energy Res.* **2019**, *43*, 1974. [CrossRef]
16. Heo, J.; Moon, H.; Chang, S.; Han, S.U.; Lee, D.E. Case Study of Solar Photovoltaic Power-Plant Site Selection for Infrastructure Planning Using a BIM-GIS-Based Approach. *Appl. Sci.* **2021**, *11*, 8785. [CrossRef]
17. Sánchez-Lozano, J.M.; Teruel-Solano, J.; Soto-Elvira, P.L.; García-Cascales, M.S. Geographical Information Systems (GIS) and Multi-Criteria Decision Making (MCDM) methods for the evaluation of solar farms locations: Case study in south-eastern Spain. *Renew. Sustain. Energy Rev.* **2013**, *24*, 544–556. [CrossRef]
18. Hernandez-Callejo, L.; Gallardo-Saavedra, S.; Alonso-Gomez, V. A review of photovoltaic systems: Design, operation and maintenance. *Sol. Energy* **2019**, *188*, 426–440. [CrossRef]
19. Ridha, H.M.; Gomes, C.; Hizam, H.; Ahmadipour, M.; Heidari, A.A.; Chen, H. Multi-objective optimization and multi-criteria decision-making methods for optimal design of standalone photovoltaic system: A comprehensive review. *Renew. Sustain. Energy Rev.* **2021**, *135*, 110202. [CrossRef]
20. Jung, J.; Han, S.U.; Kim, B. Digital numerical map-oriented estimation of solar energy potential for site selection of photovoltaic solar panels on national highway slopes. *Appl. Energy* **2019**, *242*, 57–68. [CrossRef]
21. Jiang, W.; Wang, T.; Yuan, D.; Sha, A.; Zhang, S.; Zhang, Y.; Xiao, J.; Xing, C. Available solar resources and photovoltaic system planning strategy for highway. *Renew. Sustain. Energy Rev.* **2024**, *203*, 114765. [CrossRef]
22. Ferri, C.; Ziar, H.; Nguyen, T.T.; Van Lint, H.; Zeman, M.; Isabella, O. Mapping the photovoltaic potential of the roads including the effect of traffic. *Renew. Energy* **2022**, *182*, 427–442. [CrossRef]

23. Carta, J.A.; Ramirez, P.; Velazquez, S. A review of wind speed probability distributions used in wind energy analysis: Case studies in the Canary Islands. *Renew. Sustain. Energy Rev.* **2009**, *13*, 933–955.
24. Li, J.; Zhang, Z.; Shen, B.; Gao, Z.; Pan, J. The capacity allocation method of photovoltaic and energy storage hybrid system considering the whole life cycle. *J. Clean Prod.* **2020**, *275*, 122902. [CrossRef]
25. Li, B.; Sun, H.; Lou, J.; Sun, K.; Zhang, Z.; Sun, Y. An Integration Scheme for Highway Rest Area Integrating the Distributed Photovoltaic Generation and Energy Storage. *IEEE Trans. Ind. Appl.* **2024**, *60*, 1083–1092. [CrossRef]
26. Dong, X.; Shen, J.; Liu, C.; Ma, Z.; He, Y. Simultaneous capacity configuration and scheduling optimization of an integrated electrical vehicle charging station with photovoltaic and battery energy storage system. *Energy* **2024**, *289*, 129991. [CrossRef]
27. Ozturk, Z.; Demirci, A.; Terkes, M.; Yumurtaci, R. Optimal planning of solar PV-based electric vehicle charging stations empowered by energy storage system: Feasibility and green charge potential. *Renew. Energy* **2025**, *255*, 123715. [CrossRef]
28. Li, Y.; Gao, B.; Qin, Y.; Chen, N. A hierarchical multi-objective capacity planning method for distributed energy system considering complementary characteristic of solar and wind. *Int. J. Electr. Power Energy Syst.* **2022**, *141*, 108200. [CrossRef]
29. Lv, M.; Gou, K.; Chen, H.; Lei, J.; Zhang, G.; Liu, T. Optimal Design of Wind-Solar complementary power generation systems considering the maximum capacity of renewable energy. *Energy* **2024**, *312*, 113650. [CrossRef]
30. Shi, R.; Gao, Y.; Ning, J.; Tang, K.; Jia, L. Research on highway self-consistent energy system planning with uncertain wind and photovoltaic power output. *Sustainability* **2023**, *15*, 3166. [CrossRef]
31. Wang, L.; Wang, J.; Wang, Y.; Lin, F.; Zhu, X.; Jiang, C.; Shi, R. Capacity Optimization Configuration of a Highway Ring Multi-Microgrid System Considering the Coordination of Fixed and Mobile Energy Storage. *Sustainability* **2026**, *18*, 629. [CrossRef]
32. Xia, S.; Zhang, X.; Yuan, L.; Wu, T.; Li, G.; Shahidehpour, M. An Energy Scheduling Scheme for Highway Microgrids Virtually Networked by Electric Operation and Maintenance Vehicles. *IEEE Trans. Ind. Appl.* **2024**, *60*, 1010–1022. [CrossRef]
33. Wang, B.; Lu, J.; Sha, A.M.; Jiang, W.; Liu , Z.Z.; Ke, J. Energy management strategy of integrated photovoltaic-storage-swapping on highways considering influence of photovoltaic uncertainty. *J. Traffic Transp. Eng.* **2024**, *24*, 14–30.
34. Song, Y.; Xia, M.; Yang, L.; Chen, Q.; Su, S. Multi-granularity source-load-storage cooperative dispatch based on combined robust optimization and stochastic optimization for a highway service area micro-energy grid. *Renew. Energy* **2023**, *205*, 747–762. [CrossRef]
35. Zhou, J.; Xiang, Y.; Zhang, X.; Sun, Z.; Liu, X.; Liu, J. Optimal self-consumption scheduling of highway electric vehicle charging station based on multi-agent deep reinforcement learning. *Renew. Energy* **2025**, *238*, 121982. [CrossRef]
36. Ding, R.; Rao, Z.; Li, B.; Liu, J.; Liu, X. Capacity optimization and multimode operation analysis of electric vehicle charging system powered by grid, solar and geothermal energy. *Sustain Energy Technol. Assess.* **2024**, *68*, 103851. [CrossRef]
37. Hammam, A.H.; Nayel, M.A.; Mohamed, M.A. Optimal design of sizing and allocations for highway electric vehicle charging stations based on a PV system. *Appl. Energy* **2024**, *376*, 20. [CrossRef]
38. Lin, F.; Shi, R.; Liu, X.; Jia, L.; Lee, K.Y. Energy storage capacity optimization for dual-transformer highway service areas with cross-side photovoltaic–storage–charging coordination. *Energy* **2026**, *361*, 141962. [CrossRef]
39. Lin, J.F.; Qiu, J.; Tao, Y.C.; Sun, X.Z. Planning of Electric Vehicle Charging Stations With PV and Energy Storage Using a Fuzzy Inference System. *IEEE Trans. Transp. Electrif.* **2024**, *10*, 5894–5909. [CrossRef]
40. Lu, J.A.; Zheng, W.J.; Yu, Z.W.; Xu, Z.Q.; Jiang, H.L.; Zeng, M.D. Optimizing Grid-Connected Multi-Microgrid Systems With Shared Energy Storage for Enhanced Local Energy Consumption. *IEEE Access* **2024**, *12*, 13663–13677. [CrossRef]
41. Kumar, A.; Singh, A.R.; Raghav, L.P.; Deng, Y.; He, X.N.; Bansal, R.C.; Kumar, P.; Naidoo, R.M. State-of-the-art review on energy sharing and trading of resilient multi microgrids. *iScience* **2024**, *27*, 109549. [CrossRef] [PubMed]
42. Kim, B.; Han, S.U.; Hen, J.; Jung, B. Proof-of-concept of a two-stage approach for selecting suitable slopes on a highway network for solar photovoltaic systems: A case study in South Korea. *Renew. Energy* **2020**, *151*, 366–377. [CrossRef]
43. Zhang, Y.; Liu, C.; Lei, Y.; Tang, Y.; Yu, Q.; Shen, Y.; Sun, H. An integrated algorithm for estimating regional latent heat flux and daily evapotranspiration. *Int. J. Remote Sens.* **2006**, *27*, 129–152. [CrossRef]
44. Zhang, Y.; Jiang, W.; Zhang, S.; Wang, T.; Xiao, J.; Yuan, D. Energy load forecasting of highway facilities in response to integration transportation and energy needs. *J. Traffic. Transp. Eng.* **2014**, *24*, 40–53.

Disclaimer/Publisher's Note: The statements, opinions and data contained in all publications are solely those of the individual author(s) and contributor(s) and not of MDPI and/or the editor(s). MDPI and/or the editor(s) disclaim responsibility for any injury to people or property resulting from any ideas, methods, instructions or products referred to in the content.